Generated using the official AMS LaTeX template—two-column layout. FOR AUTHOR USE ONLY, NOT FOR SUBMISSION!

JOURNAL OF THE ATMOSPHERIC SCIENCES

arXiv:1810.11105v1 [physics.ao-ph] 25 Oct 2018

Hadley cell emergence and extent in axisymmetric, nearly inviscid, planetary atmospheres

SPENCER A. HILL*

Department of Atmospheric and Oceanic Sciences, University of California, Los Angeles and Division of Geological and Planetary Sciences, California Institute of Technology, Pasadena, California

SIMONA BORDONI

Division of Geological and Planetary Sciences, California Institute of Technology, Pasadena, California

JONATHAN L. MITCHELL

Department of Earth, Planetary, and Space Sciences, and Department of Atmospheric and Oceanic Sciences, University of California, Los Angeles

ABSTRACT

The authors consider constraints from axisymmetric, nearly inviscid theory on Hadley cell emergence and extent in dry planetary atmospheres. Existing versions of the well-known Hide's constraint relating Hadley cell emergence to the distributions of absolute angular momentum (M) and the vertical component of absolute vorticity (η) are unified, amounting to any of $M > \Omega a^2$, $M < 0$, or $f\eta < 0$ occurring at any latitude. The $M < 0$ condition coincides with the gradient-balanced zonal wind in radiative convective equilibrium (RCE; $u_{\rm rce}$) becoming non-real valued. The resulting angular momentum conserving (AMC) circulation must span all latitudes where any of these conditions are met or where $u_{\rm rce}$ exceeds the AMC zonal wind ($u_{\rm amc}$) corresponding to planetary angular momentum at the latitude of the circulation's ascent branch ($\varphi_{\rm a}$), but a generally valid prognostic theory for $\varphi_{\rm a}$ remains elusive. Nevertheless, given a diagnosed $\varphi_{\rm a}$, the $u_{\rm rce} > u_{\rm amc}$ condition provides a simple explanation for why cross-equatorial Hadley circulations typically extend as far into the winter- as the summer hemisphere. The classical "equal-area" models predict $\varphi_{\rm a}$ but typically must be solved numerically and always predict $\varphi_{\rm a}$ at or poleward of the RCE forcing maximum ($\varphi_{\rm m}$) for $\varphi_{\rm m} \neq 0$. In an idealized dry general circulation model, a pole-to-pole cross-equatorial Hadley cell emerges if the corresponding RCE state meets some combination of these extent criteria over the entire summer hemisphere. Conversely, the cell edge and $\varphi_{\rm a}$ sit far equatorward of $\varphi_{\rm m}$ if those criteria are not satisfied near $\varphi_{\rm m}$.

1. Introduction

A compelling explanation for the prevalence of zonally symmetric, low-latitude meridional overturning circulations — Hadley cells — across planetary atmospheres comes from Hide's constraint: isolated extrema in angular momentum away from the surface are forbidden in steady, axisymmetric atmospheres with nonzero viscosity above the planetary boundary layer (Hide 1969; Schneider 1977). If any such extrema were to be generated by the gradient-balanced zonal wind field that would otherwise exist in a state of latitude-by-latitude radiative convective equilibrium (RCE) given the top-of-atmosphere radiative forcing and other boundary conditions, a meridional overturning circulation must emerge to smooth them away. Violation of Hide's constraint occurs most easily near the equator, requiring only a nonzero meridional first derivative or negative second derivative in the equatorial RCE equivalent potential temperature averaged over some depth of the troposphere (Held and Hou 1980; Lindzen and Hou 1988). Given meridional variations in the incidence angle of stellar radiation on spherical planets, such violations are difficult to avoid (Schneider 2006).

Any latitude where Hide's constraint is violated is said to be supercritically forced, and supercritical forcing can also occur away from the equator in ways discussed further below. But while the existence of supercritical forcing at any latitude necessitates the *emergence* of a Hadley circulation (comprising one or more distinct overturning cells), it does not fully constrain the resulting circulation's meridional *extent*. In axisymmetric atmospheres where viscosity is nonzero but small above a strongly damped boundary layer, the Hadley cells are usefully described by the angular momentum conserving (AMC) model: the Hadley circulation homogenizes angular momentum within its confines and must span all latitudes where the local RCE angular momentum value exceeds the circula-

*Corresponding author address: Spencer Hill, UCLA Atmospheric and Oceanic Sciences, Box 951565, Los Angeles, CA 90095-1565
E-mail: shill@atmos.ucla.edu

tion's. This lower bound on Hadley circulation extent explains the qualitative diversity of Hadley cells in thin-shell atmospheres[1] across the solar system — confined to low latitudes on Earth vs. planetary in scale on small radius and/or slowly rotating bodies like Venus (Gierasch 1975), Mars (Haberle et al. 1993), and Titan (Mitchell and Lora 2016).

Assuming the circulation's ascending branch is narrow and features negligible zonal flow, the value of angular momentum that the AMC circulation homogenizes is set by the value of planetary angular momentum at the latitude of the ascending branch, φ_a. But what determines φ_a? AMC theory provides a diagnostic for φ_a that has proven useful on Earth, namely that φ_a is coincident with the global maximum in some indicator of the column-integrated thermodynamic tracer[2]. However, Faulk et al. (2017) present simulations in an Earth-like idealized aquaplanet in which near-surface moist static energy maximizes at the summer pole during solsticial seasons or under time invariant solsticial forcing — ~60° poleward of the Hadley circulation's summer poleward edge located at ~30°N (see their Figure 3). Better theoretical understanding of the conditions under which such vast separations can occur is needed and, we argue, will be easier attained if they can be generated in more idealized contexts (Held 2005; Jeevanjee et al. 2017).

Even in cases where the thermal maximum explanation for φ_a holds, it requires knowledge of the dynamically equilibrated thermal field, i.e. it cannot be predicted from the RCE state. A prognostic theory for φ_a (as well as the other AMC cell edges) does emerge from the well known "equal-area" arguments requiring continuity of temperature and conservation of energy spanning each AMC cell (Held and Hou 1980; Lindzen and Hou 1988). But the utility of the equal-area predictions across planetary atmospheres has been little explored, particularly for cases where the radiative forcing maximizes off the equator.

Before proceeding, it is fair to question the relevance of axisymmetric arguments to eddying atmospheres. On Earth, baroclinic eddies modulate the Hadley cells' extent and overturning strength (Walker and Schneider 2005; Korty and Schneider 2008; Levine and Schneider 2015; Singh and Kuang 2016; Singh et al. 2017) and decelerate the zonal wind of the annual mean Hadley cells well below the AMC limit (Walker and Schneider 2006). Nevertheless, large expanses of cross-equatorial, zonally confined monsoons and zonal mean Hadley cells during solsticial seasons do reliably approach the AMC limit (e.g. Schneider and Bordoni 2008; Bordoni and Schneider 2008, 2010).[3] Accordingly, axisymmetric theory (in its modern "convective quasi-equilibrium" form appropriate for moist, convecting atmospheres, c.f. Emanuel 1995) retains validity in — and is the dominant existing theoretical paradigm for — these contexts (e.g. Nie et al. 2010). The importance of baroclinic eddies diminishes as either planetary rotation rate or radius decrease, leading to a "global Tropics" regime once the Rossby radius of deformation exceeds the planetary scale (Williams and Holloway 1982; Mitchell et al. 2006; Faulk et al. 2017). In addition to the solar system's slow rotators of Venus and Titan, in all likelihood this characterizes many "habitable zone" exoplanets identified already or likely to be identifiable by existing and planned telescope missions, due to orbital dynamical constraints (e.g. Showman et al. 2014).

These considerations compel the present study, in which we assess the utility of nearly inviscid, axisymmetric theory in characterizing the emergence and extent of Hadley circulations for thin-shell atmospheres for planetary bodies with Hadley cells ranging from comparable to Earth's to planetary in scale. Our primary goals with respect to existing axisymmetric theory are twofold: first, to clarify those aspects that we have found prone to misunderstanding, and, second, to newly describe some implications that we have not found noted before. One such implication that emerges without appeal to the equal-area arguments is that a cross-equatorial AMC cell can almost always be expected to extend as far or farther into the winter hemisphere as into the summer hemisphere.

The theory of Hadley cell emergence is addressed in Section 2 and of extent in Section 3, the latter also discussing controls on the locations of the ascent branch. The resulting ideas are tested via numerical simulations presented in Section 4 in an axisymmetric, idealized dry GCM. We conclude with a summary (Section 5) and discussion (Section 6) of these results. For the sake of analytical tractability, we focus throughout on dry, axisymmetric, Boussinesq atmospheres under time invariant radiative forcing for which the resulting RCE potential temperatures (and corresponding gradient-balanced zonal winds) are known analytically. We show below (in Section 3) that the Boussinesq system yields results effectively isomorphic to those of atmospheres obeying convective quasi-equilibrium (CQE; Emanuel 1995). The study of dry atmospheres is also of direct relevance to effectively dry atmospheres such as on present-day Mars and in Earth's deep past during so-called "snowball" events (Caballero

[1] We are considering nearly inviscid theory in the thin-shell limit (wherein vertical variations in the moment arm are taken as negligible compared to meridional variations) appropriate for terrestrial bodies but not the gas giants. See e.g. Schneider and Liu (2009) and O'Neill and Kaspi (2016) for consideration of angular momentum dynamics in deep atmospheres.

[2] I.e. troposphere-averaged potential temperature in dry atmospheres (Lindzen and Hou 1988), subcloud moist entropy (Emanuel 1995), or near-surface moist static energy (Privé and Plumb 2007a) in moist atmospheres obeying "convective quasi equilibrium" (Emanuel et al. 1994).

[3] Another concern in applying steady axisymmetric theory to seasonally varying atmospheres is that axisymmetric general circulation model simulations can require hundreds of days — i.e. well beyond Earth's seasonal timescale — for the Hadley circulation to reach a statistically state (Plumb and Hou 1992; Fang and Tung 1999).

et al. 2008). We heavily utilize the results of Held and Hou (1980), Lindzen and Hou (1988), Plumb and Hou (1992), and Emanuel (1995) and refer to them henceforth as HH80, LH88, PH92, and E95, respectively.

2. Hadley cell emergence

This section presents Hide's constraint more formally, considers both leading-order properties and more subtle aspects of the gradient balance condition for an axisymmetric RCE state, and delineates three conditions of the RCE state, each independently constituting a sufficient condition for the emergence of a Hadley circulation.

a. Hide's constraint

We present the traditional form of Hide's constraint for axisymmetric atmospheres first and the generalized form introduced by E95 second. Consider the free troposphere of an axisymmetric atmosphere in steady state in which viscosity is nonzero, such that momentum is diffused down-gradient. The time-mean zonal momentum equation (incorporating the incompressible continuity equation $\nabla \cdot \mathbf{v} = 0$) is

$$\overline{\mathbf{v}} \cdot \nabla \overline{M} = \nabla \cdot \left(\nu \nabla \overline{M} \right), \tag{1}$$

where $M = a\cos\varphi(\Omega a \cos\varphi + u)$ is absolute angular momentum per unit mass, a is planetary radius, φ is latitude, Ω is the planetary rotation rate, u is zonal velocity, overbars denote temporal averages, ν is the kinematic viscosity, and $\mathbf{v} = (v, w)$ with v the meridional velocity and w the vertical velocity.[4]

In atmospheres characterized by (1), Hide's constraint amounts to a prohibition on isolated extrema (i.e. points with zero first derivative but nonzero second derivative) in $\overline{M}$. Mathematically, at any such an extremum, $\nabla \overline{M} = \mathbf{0}$, so that the left-hand side of (1) must vanish but not the right-hand side. Physically, the diffusion that acts to flatten out the hypothetical extremum would have to be balanced by momentum flux convergence for a maximum (divergence for a minimum), which would require time-mean mass convergence (divergence for a minimum), and this would violate conservation of mass.[5] Only at the surface, where frictional stress can balance the diffusive term, can an extremum occur.

Because planetary angular momentum takes its maximal value of Ωa^2 at the equator, it follows that *any* equatorial $u > 0$ above the boundary layer will violate Hide's constraint. And because planetary angular momentum takes its minimal value of zero at either pole, it follows that any $u < 0$ at either pole would also violate Hide's constraint; however, at the poles zonal wind (i.e. wind perpendicular to meridians) must vanish on geometric grounds since meridians converge there. Away from the poles, $M = 0$ corresponds to $u = -\Omega a \cos\varphi$, corresponding on Earth to extremely strong easterlies at low latitudes (exceeding 400 m s^{-1} near the equator), but to more plausibly attainable values at high latitudes and at low latitudes in other planetary settings discussed below.

Away from the equator and poles, Hide's constraint is often more usefully phrased in terms of vorticity. At an isolated extremum in any field, the field's vertical and meridional derivatives vanish. The meridional derivative of angular momentum is proportional to the vertical component of absolute vorticity: $\partial_\varphi M = -(a^2 \cos\varphi)\eta$, where $\eta = f + \zeta$ is the vertical component of absolute vorticity (referred without confusion hereafter simply as absolute vorticity), $f = 2\Omega \sin\varphi$ is the planetary vorticity (i.e. the Coriolis parameter), and $\zeta = -(a\cos\varphi)^{-1}\partial_\varphi(u\cos\varphi)$ is the relative vorticity. As such, a sign change in η within a hemisphere signals the existence of extrema in M (PH92).

E95 extend this vorticity-based expression of Hide's constraint to non-axisymmetric and/or purely inviscid atmospheres. Consider the vorticity equation

$$\frac{\partial \zeta}{\partial t} = -\mathbf{u} \cdot \nabla_\mathrm{h}(f+\zeta) - w\frac{\partial \zeta}{\partial z} - (f+\zeta)\nabla_\mathrm{h} \cdot \mathbf{u} + \mathbf{k} \cdot \left(\frac{\partial \mathbf{u}}{\partial z} \times \nabla_\mathrm{h} w \right) - \mathcal{D} = 0, \tag{2}$$

where $\mathbf{u} = (u, v)$, ∇_h is the horizontal divergence operator, $\mathcal{D}$ is a damping term whose functional form is irrelevant insofar as it vanishes when ζ vanishes (as it should), and in zonally varying atmospheres a $+\partial_x v$ term is added to ζ. Suppose there exists some level at which vertical velocity vanishes at all latitudes and longitudes (the tropopause being a plausible candidate, insofar as it occurs at a fixed level in RCE as argued by Caballero et al. 2008). At that level, all terms of (2) featuring w are zero, and the remaining terms on the right hand side also vanish if $\eta = f + \zeta = 0$. In that case, $\partial_t \eta = \partial_t \zeta = 0$: $\eta = 0$ is a stationary point, meaning that it is impossible for absolute vorticity to evolve in time from one sign to another. Thus, given an initial resting state (or one with sufficiently weak horizontal shears that η everywhere takes the sign of f), a subsequent state with $f\eta < 0$ is impossible.

Figure 1 visualizes this $f\eta < 0$ condition by showing the potential temperature, zonal wind, angular momentum, and absolute vorticity fields corresponding to the depth-averaged forcing of PH92 (their Eq. 9), which comprises

[4] Neglected in (1) is the divergence of eddy momentum fluxes, $\nabla \cdot \overline{M'\mathbf{v}'}$, where primes denote deviations from the time-mean. In non-axisymmetric atmospheres, zonally asymmetric eddies can generate interior extrema in the angular momentum field, the most notorious example being a westerly, "superrotating" jet in the equatorial troposphere, through a variety of mechanisms (e.g. Schneider and Liu 2009; Caballero and Huber 2010; Mitchell and Vallis 2010; Wang and Mitchell 2014). In simulations of axisymmetric atmospheres (including those we present in Section 4), propagating symmetric instabilities are ubiquitous and could theoretically do the same, but HH80 provides qualitative arguments that this is unlikely (but see also Kirtman and Schneider 2000). We continue to neglect eddy influences in all that follows.

[5] See Appendix A of PH92 for a formal proof.

an isolated but finite width forcing region centered at the latitude φ_m (namely, 30° wide and centered at 25°N), for successively larger values of the forcing maximum. With no maximum present (dashed black curves), $u_{rce} = 0$ everywhere, and M and η take their planetary values. Introducing a weak forcing maximum (blue curves) generates easterlies on the maximum's equatorward side and westerlies on the poleward side. The easterlies bend the M curve down, and the westerlies bend the M curve up, but not enough to generate any extrema in M: η retains its original sign everywhere, and the forcing is subcritical. Increasing the magnitude of the forcing maximum causes the easterlies and westerlies to intensify, eventually enough to generate $\eta = 0$ at a point slightly equatorward of φ_m (gray curves). A forcing maximum that is any stronger is supercritical (red curves): M develops a minimum equatorward and a maximum poleward of φ_m, between which η has changed sign.

b. *Gradient wind balance in radiative convective equilibrium*

Latitude-by-latitude RCE implies $v = w = 0$, in which case combining the meridional momentum and hydrostatic balance equations leads to zonal wind and potential temperatures (u_{rce} and θ_{rce}, respectively) in gradient wind balance:

$$\frac{\partial}{\partial z}\left(\frac{\tan\varphi}{a}u_{rce}^2 + f u_{rce}\right) = -\frac{g}{a\theta_0}\frac{\partial \theta_{rce}}{\partial \varphi}, \qquad (3a)$$

where θ_0 is the Boussinesq reference potential temperature.[6] Assuming drag in the boundary layer is large enough that the surface zonal wind is negligible[7], the integral of (3a) from the surface to some height z yields

$$\frac{\tan\varphi}{a}u_{rce}^2(z) + f u_{rce}(z) + \frac{gz}{a\theta_0}\frac{\partial \hat{\theta}_{rce}}{\partial \varphi} = 0, \qquad (3b)$$

where $\hat{\theta}$ is the average of θ between the surface and z. (3b) is a quadratic equation for u_{rce} that can be solved directly. Choosing the positive root (since it corresponds to $u_{rce} = 0$ at the surface as required), this is

$$u_{rce} = \Omega a \cos\varphi \left[\sqrt{1 - \frac{1}{\cos\varphi \sin\varphi}\frac{gz}{\Omega^2 a^2 \theta_0}\frac{\partial \hat{\theta}_{rce}}{\partial \varphi}} - 1\right]. \qquad (4)$$

Away from the equator, if $\partial_\varphi \hat{\theta}_{rce} = 0$ then $u_{rce} = 0$. At the equator, if $\partial_\varphi \hat{\theta}_{rce} = 0$, then $\lim_{\varphi\to 0} u_{rce}$ is indeterminate and is thus solved using L'Hôpital's rule to give

$$u_{rce}(\phi{=}0, \partial_\varphi \hat{\theta}_{rce}{=}0) = \Omega a \left[\sqrt{1 - \frac{gz}{\Omega^2 a^2 \theta_0}\frac{\partial^2 \hat{\theta}_{rce}}{\partial \varphi^2}} - 1\right],$$

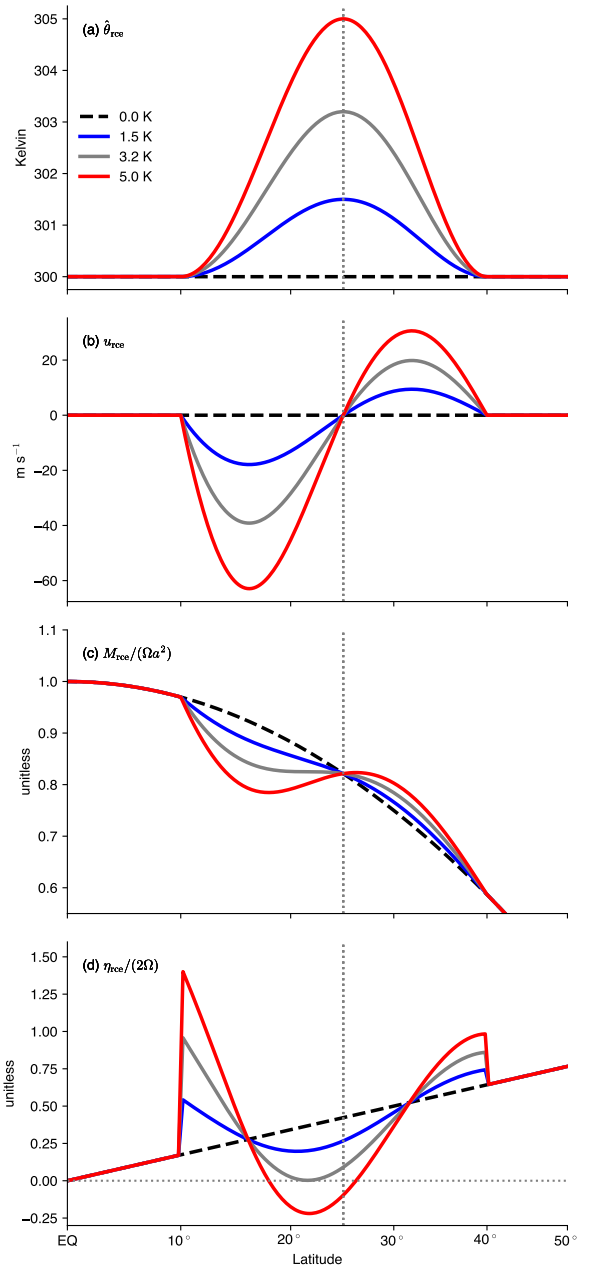

FIG. 1. RCE profiles corresponding to the forcing used by Plumb and Hou (1992, their Eq. 9), which comprises uniform $\hat{\theta}_{rce}$ at all latitudes other than a "bump" centered on 25°N (indicated by the vertical gray dotted line) and 30° wide, of (a) column-averaged potential temperature (in Kelvin), (b) zonal wind (in m s^{-1}), (c) absolute angular momentum normalized by the planetary angular momentum at the equator, and (d) absolute vorticity normalized by twice the planetary rotation rate, for different magnitudes of the forcing maximum as indicated by the legend in (a). The horizontal dotted gray line in (d) marks the zero line.

[6] The perhaps more familiar thermal wind relation follows from geostrophic, rather than gradient balance — i.e. using (3a) but omitting the nonlinear metric term $(\tan\varphi/a)u_{rce}^2$.

[7] Or, more formally, assuming lower boundary conditions of $\nu\partial_z u = Cu$, $\nu\partial_z v = Cv$, where C is a constant drag coefficient, c.f. Eq. 3 of HH80.

from which it can be seen that any equatorial maximum in potential temperature with nonzero second derivative violates Hide's constraint at the equator. If the second derivative is also zero, zonal flow at the equator will remain zero, but this is unlikely in the annual mean for Earth-like orbits (as argued more formally by Schneider 2006). Flatter annual-mean profiles become more relevant for planets with larger orbital obliquities (with the poles receiving more annual mean insolation than the equator for orbits with obliquities $\gtrsim 55°$; e.g. Linsenmeier et al. 2015), although in those cases the annual mean Hadley cells are likely the small residual of very strong, seasonally reversing cells that rarely approach cross-equatorial symmetry.

As noted by Fang and Tung (1996), a real-valued solution to (4) does not exist if the quantity within the square root operator is negative, in which case the physical interpretation for a steady state is that the advective terms must be nonzero, i.e. that RCE cannot be sustained. Interestingly, the minimum real solution is $u_{\rm rce} = -\Omega a \cos\varphi$, which as noted above is the value for which $M = 0$ at all latitudes. We lack at present a satisfying explanation for this coincidence of the $M < 0$ manifestation of Hide's constraint (which derives from the zonal momentum equation) with the gradient-balanced wind (which derives from the continuity, hydrostatic, and meridional momentum equations). In contrast, the $u_{\rm rce}$ value corresponding to the $M = \Omega a^2$ condition is not mathematically coincide with any mathematically unique property of $u_{\rm rce}$.

c. *Sufficient conditions for the violation of Hide's constraint*

In summary, a Hadley circulation must emerge in an axisymmetric atmosphere with nonzero viscosity whose RCE state meets any one of the following three conditions at any latitude:

1. $M > \Omega a^2$ (global maximum in M)
2. $M < 0$ (global minimum in M and complex-valued $u_{\rm rce}$)
3. $f\eta < 0$ (local extrema in M and unrealizable sign change in η)

Henceforth, we use $M > \Omega a^2$, $M < 0$, and $f\eta < 0$ respectively as notational shorthand for these conditions.

It can be useful to recast each condition purely in terms of the thermal field $\hat{\theta}_{\rm rce}$, which is often known or imposed directly in simulations, rather than in terms of $u_{\rm rce}$ or η, since $u_{\rm rce}$ must be inferred from $\hat{\theta}_{\rm rce}$ via gradient balance, and η must be subsequently computed from $u_{\rm rce}$. For the $M > \Omega a^2$ and $M < 0$ conditions with $\varphi \neq 0$, these are

$$\left.\frac{1}{\theta_0}\frac{\partial \hat{\theta}_{\rm rce}}{\partial \varphi}\right|_{M=\Omega a^2} = -\frac{\Omega^2 a^2}{gH}\frac{\sin^3\varphi}{\cos^3\varphi}\left(1+\cos^2\varphi\right), \tag{5a}$$

$$\left.\frac{1}{\theta_0}\frac{\partial \hat{\theta}_{\rm rce}}{\partial \varphi}\right|_{M=0} = \frac{\Omega^2 a^2}{gH}\sin\varphi\cos\varphi, \tag{5b}$$

where H is the tropopause height. The corresponding $f\eta < 0$ expression was introduced by PH92 (their Eq. 8; see Eq. 10 of E95 for the CQE analog) and may be written

$$C_{\rm ph92} = 4\Omega^2 a^2 \cos^3\varphi \sin\varphi + \frac{gH}{\theta_0}\frac{\partial}{\partial\varphi}\left(\frac{\cos^3\varphi}{\sin\varphi}\frac{\partial \hat{\theta}_{\rm rce}}{\partial\varphi}\right). \tag{5c}$$

$C_{\rm ph92} > 0$ corresponds to supercritical forcing in the Northern Hemisphere and subcritical forcing in the Southern Hemisphere (signs that are the same as for η itself).

3. Hadley cell extent and ascent branch location

Supposing that $u_{\rm rce}$ and $\hat{\theta}_{\rm rce}$ meet one or more of the above sufficient conditions for Hadley cell emergence, over what latitudes does the resulting overturning circulation extend, and where is its ascending branch located? This section considers arguments based on successively more stringent constraints: those stemming directly from the emergence conditions, from the AMC model, and from the equal-area model. We consider each for general $\hat{\theta}_{\rm rce}$ profiles and as applied to the canonical $\hat{\theta}_{\rm rce}$ profiles of LH88 and HH80:

$$\frac{\hat{\theta}_{\rm lh88}}{\theta_0} = 1 + \frac{\Delta_{\rm h}}{3}\left[1 - 3(\sin\varphi - \sin\varphi_{\rm m})^2\right], \tag{6a}$$

where $\Delta_{\rm h}$ is an imposed fractional equator-to-pole temperature contrast, and the forcing maximizes at the latitude $\varphi_{\rm m}$. For $\varphi_{\rm m} = 0$, this reduces to

$$\frac{\hat{\theta}_{\rm hh80}}{\theta_0} = 1 + \frac{\Delta_{\rm h}}{3}\left[1 - 3\sin^2\varphi\right], \tag{6b}$$

which is equivalent to the vertically-averaged "Held-Suarez" forcing used ubiquitously in theoretical and numerical studies of Earth's annual mean circulation (Held and Suarez 1994). Using (6a) in (4), the corresponding $u_{\rm rce}$ fields are

$$u_{\rm rce,lh88} = \Omega a \cos\varphi\left[\sqrt{1 + 2R\left(1 - \frac{\sin\varphi_{\rm m}}{\sin\varphi}\right)} - 1\right], \tag{7a}$$

where

$$R = \frac{gH\Delta_{\rm h}}{\Omega^2 a^2}$$

is the thermal Rossby number, and, for $\varphi_{\rm m} = 0$,

$$u_{\rm rce,hh80} = \Omega a \cos\varphi\left[\sqrt{1+2R} - 1\right]. \tag{7b}$$

a. Constraints from the emergence criteria

At the very least, the Hadley circulation must span all latitudes meeting any of the $M > \Omega a^2$, $M < 0$, or $f\eta < 0$ conditions. But this lower bound in not always especially useful, for example in the PH92 case: c.f. Figure 1, the supercritical forcing shown generates no global M extrema (although sufficiently strong forcing would) and an $f\eta < 0$ range spanning only ~18-26°N, whereas the corresponding PH92 simulation (for which the forcing is stronger and the supercritical region spans ~12-29°N; not shown) features a Hadley circulation spanning ~25°S-30°N (c.f. their Fig. 5a).

Under the HH80 forcing, neither the $M < 0$ nor $f\eta < 0$ criteria are met at any latitude. This is demonstrated by the solid red curves in Figure 2, which show (a) $\hat{\theta}_{\rm rce}$, (b) $u_{\rm rce}$, (c) M, and (d) η for (6b) with Earth's values of g, Ω, and a, $H = 10$ km, and $\Delta_{\rm h} = 1/3$, yielding $R \approx 0.15$ [the other plotted elements will be discussed further below]. $u_{\rm rce}$ and $M_{\rm rce}$ are maximal at the equator and decrease monotonically toward zero at either pole. The meridional shear makes $f\eta$ *more* positive than it would be in a resting atmosphere [shown as the pink dashed curve in panel (d)]. This in fact holds for the more general forcing of $\hat{\theta}_{\rm rce}/\theta_0 = c_1 + c_2 \cos^n \varphi$, where c_1 and c_2 are constants and $n \geq 2$ is a positive integer [of which (6b) is a special case with $c_1 = 1 - 2\Delta_{\rm h}/3$, $c_2 = \Delta_{\rm h}$, and $n = 2$]. Applying (5c) to this yields

$$C_{{\rm ph92},\cos^n\varphi} = -\sin\varphi\cos^3\varphi\left[4\Omega^2a^2 + n(n+2)c_2gH\cos^{n-2}\varphi\right].$$

All of the terms within the square brackets are positive, which combined with the leading $-\sin\varphi$ term corresponds to $f\eta \geq 0$ at all latitudes.

For the LH88 forcing, Figure 3 repeats Figure 2 but with $\varphi_{\rm m} = 6°$. Westerlies are sufficiently strong from the winter subtropics to the equator and in the ~10°-wide span just poleward of $\varphi_{\rm m}$ to generate $M > \Omega a^2$. Moving across the equator toward the summer pole, $\partial_\varphi \hat{\theta}_{\rm rce} > 0$ causes $u_{\rm rce}$ to flip to non-real values that violate the $M < 0$ constraint, though only very near the equator. But the meridional shear is sufficiently large poleward of there to generate an $f\eta < 0$ region spanning another ~10°. These spans are indicated by the three lower-most horizontal lines at the top of panel (a) as indicated by the legend (likewise for Figure 2 but with the $M < 0$ and $f\eta < 0$ conditions omitted).

More formally, (7a) implies $M < 0$ where

$$\frac{2R}{1+2R} > \frac{\sin\varphi}{\sin\varphi_{\rm m}}. \tag{8}$$

The left-hand side of (8) is at most unity, while the right-hand side is <1 for $0 < \varphi < \varphi_{\rm m}$ and ≥1 for $\varphi \geq \varphi_{\rm m}$, guaranteeing some finite latitude range in the summer hemisphere for which no RCE solution exists. For very large R, the left-hand side approaches unity, such that the $M < 0$ constraint is violated essentially all the way to $\varphi_{\rm m}$, and the circulation is certain to extend at least to the vicinity of $\varphi_{\rm m}$.

For the $f\eta < 0$ condition, the absolute vorticity field corresponding to (7a) is

$$\eta_{\rm rce,lh88} = \Omega\sqrt{1+2R\left(1-\frac{\sin\varphi_{\rm m}}{\sin\varphi}\right)} \times\left(2\sin\varphi - \frac{\cos^2\varphi}{\sin^2\varphi}\frac{R\sin\varphi_{\rm m}}{1+2R\left(1-\frac{\sin\varphi_{\rm m}}{\sin\varphi}\right)}\right). \tag{9a}$$

Evaluated at $\varphi_{\rm m}$, this becomes

$$\eta_{\rm rce,lh88}(\varphi{=}\varphi_{\rm m}) = 2\Omega\sin\varphi_{\rm m}\left(1-\frac{R}{2}\frac{\cos^2\varphi_{\rm m}}{\sin^2\varphi_{\rm m}}\right), \tag{9b}$$

which shows that $f\eta(\varphi{=}\varphi_{\rm m}) < 0$ if $\tan^2\varphi_{\rm m} < R/2$, or $\varphi_{\rm m} < \sqrt{R/2}$ in the small-angle limit. For the original LH88 case with $\varphi_{\rm m} = 6° \approx 0.1$ radians and $R \approx 0.1$, it follows that $\sqrt{R/2} \approx 0.2$, and thus the $f\eta < 0$ condition is met at $\varphi_{\rm m}$, as shown in Figure 3. Figure 4 shows (9b) as a function of $\varphi_{\rm m}$, both with and without thee small angle approximation. As the forcing maximum moves poleward, a larger R is required to ensure the circulation extends at least to $\varphi_{\rm m}$.

b. Constraints from the AMC Hadley cell model

Before describing the AMC Hadley cell model, we note that Hide's constraint holds for any nonzero viscosity, and in atmospheres with sufficiently large ν the appropriate model for Hadley cells that emerge is the viscous, linear one (Schneider and Lindzen 1977; Fang and Tung 1994). But as a model for most terrestrial planets including Earth, the nearly inviscid, angular momentum conserving model is more appropriate; see Fang and Tung (1994) for a formal treatment of this regime separation based on the relative values of the Ekman and Rossby numbers. As stressed by HH80, the nearly inviscid solution cannot be obtained as the limiting case of the viscous solution as $\nu \to 0^+$. We only consider the inviscid, AMC model henceforth.

1) CONCEPTUAL BASIS FOR THE AMC HADLEY CELL MODEL

If zonal wind is negligible at some latitude $\varphi_{\rm a}$, then the angular momentum at that latitude is the planetary value, $\Omega a^2\cos^2\varphi_{\rm a}$. Other latitudes will share this value if zonal wind follows the AMC profile given by, c.f. LH88,

$$u_{\rm amc} = \Omega a\cos\varphi\left(\frac{\cos^2\varphi_{\rm a}}{\cos^2\varphi} - 1\right). \tag{10}$$

The blue curves in Figures 2(b) and 3(b) show $u_{\rm amc}$ for $\varphi_{\rm a} = 0°$ and $\varphi_{\rm a} = 21.2°$N, respectively (the latter value determined based on the equal-area model as discussed below). For any $\varphi_{\rm a}$, $u_{\rm amc}$ vanishes at $\varphi_{\rm a}$, is mirror symmetric

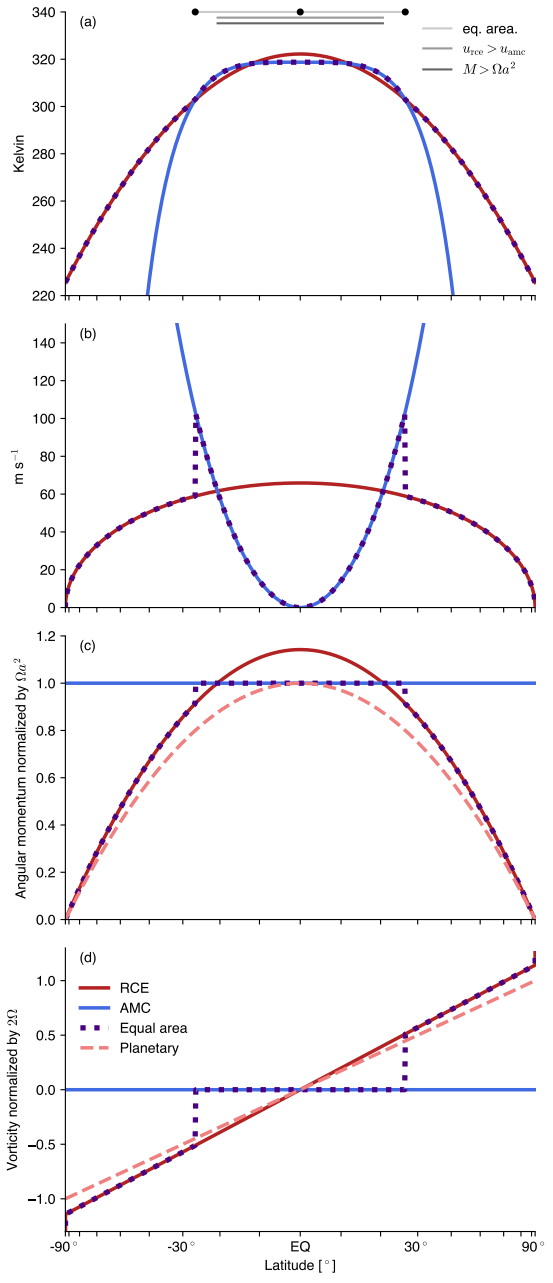

FIG. 2. Values of (a) column-averaged potential temperature (in Kelvin), (b) zonal wind (in m s^{-1}), (c) absolute angular momentum normalized by Ωa^2, and (d) absolute vorticity normalized by 2Ω, each corresponding to (solid red) the RCE state, (solid blue) the AMC solution, (dotted purple) the equal-area solution, and (c and d only, dashed pink) the planetary value, as a function of latitude (horizontal axis, with $\sin\varphi$-spacing), where the RCE forcing is given by (6a) with $\varphi_{\rm m} = 0$. Horizontal lines at the top of (a) signify Hadley cell extent markers according to the legend in (a), with the three black dots corresponding to the cell edges of the equal area solution.

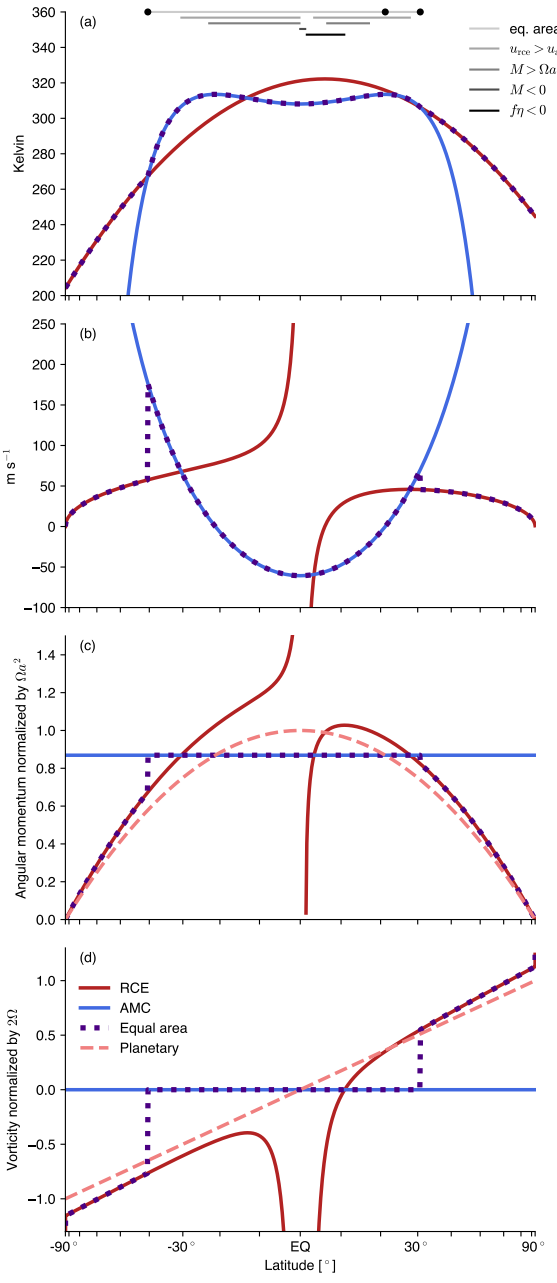

FIG. 3. Same as Fig. 2, but with the RCE forcing is given by (6a) with $\varphi_{\rm m} = 6$, and with two additional cell extent metrics in (a) as noted in the legend (both were not met at any latitude in the $\varphi_{\rm m} = 0$ case). Note that not all vertical axis spans are identical to the corresponding ones of Fig. 2.

about the equator, and increases monotonically toward either pole from a minimum value at the equator. For $\varphi_{\rm a} \neq 0$, $u_{\rm amc}$ is also zero at $-\varphi_{\rm a}$, easterly between $-\varphi_{\rm a}$ and $\varphi_{\rm a}$, and westerly poleward thereof. Unless $\varphi_{\rm a}$ is located at either pole (corresponding to the $M = 0$ case noted previously), $u_{\rm amc} \to +\infty$ at the poles. Blue curves in Figures 2(c,d) and

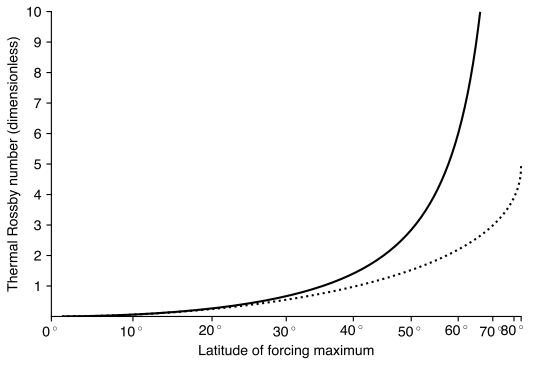

FIG. 4. Values of (horizontal axis) φ_m and (vertical axis) thermal Rossby number for which RCE absolute vorticity at φ_m corresponding to the LH88 forcing profile is zero. The solid black curve is the full solution, and the dotted black curve is the small-angle limit. Values above/to the left of the solid curve correspond to $f\eta < 0$ at φ_m, thereby ensuring a circulation that extends to at least φ_m.

3(c,d) show that M is indeed constant and thus $\eta = 0$ (both by construction).

The AMC model for the Hadley cells (HH80, LH88) assumes that ascent out of the boundary layer (in which strong surface drag imposes $u \approx 0$) occurs in a narrow band that can be characterized by a single latitude, φ_a, and that the entire Hadley circulation takes this value in the free troposphere (since viscosity is negligible there). The circulation's zonal wind field therefore must be given by (10). In reality, ascent will occur over some finite latitudinal width, within which convective momentum mixing could be non-negligible (Schneider and Lindzen 1977; Schneider 1977), although the presumably weak vertical shear there makes it not obviously a large term (c.f. Held and Hoskins 1985). Conversely, presumably large shears at the circulation's poleward edges can make the viscous term large there even for small values of η.[8]

Even if these caveats can be ignored, using the AMC model prognostically requires a theory for φ_a given the RCE values. As noted above, it is not generally the case that $\varphi_a \approx \varphi_m$. Even for $\varphi_m = 0$, off-equatorial, double ITCZs often emerge in numerical simulations such that $\varphi_a \neq 0$ (e.g. Satoh 1994). For $\varphi_m \neq 0$, φ_a can be well equatorward of φ_m if the thermal forcing is sufficiently weak and/or φ_m is sufficiently poleward. The $M > \Omega a^2$, $M < 0$, $f\eta < 0$ conditions combined provide a lower bound on the extent of the overall circulation, but in principle φ_a can occur anywhere within that span, constituting the boundary between summer and winter cells. Even in the case of a single, cross-equatorial cell (for which φ_a necessarily is also the cell edge in the summer hemisphere), the simulations we present below indicate that φ_a can occur well poleward of these criteria. A very promising diagnostic approach in these cases being developed by Martin Singh (pers. comm.) is relating the cell edge to the condition of neutrality to slantwise convection (c.f. Emanuel 1986).

2) AMC THERMAL PROFILES

The troposphere-averaged potential temperature field of the AMC circulation, $\hat{\theta}_{amc}$, is that in gradient balance with u_{amc} for a given φ_a. The case with $\varphi_a = 0$ was solved by HH80 (their Eq. 12) and generalized to $\varphi_a \neq 0$ by LH88 (their Eq. 7). The latter is

$$\frac{\hat{\theta}(\varphi) - \hat{\theta}_a}{\theta_0} = -\frac{\Omega^2 a^2}{2gH} \frac{(\cos^2\varphi_a - \cos^2\varphi)^2}{\cos^2\varphi}, \tag{11a}$$

where $\hat{\theta}_a$ is the value of $\hat{\theta}$ at φ_a. In a CQE rather than a Boussinesq atmosphere, this becomes (c.f. E95 Eq. 11)

$$\theta_b = \theta_{ba} \exp\left[-\frac{\Omega^2 a^2}{2c_p(T_s - T_t)} \frac{(\cos^2\varphi_a - \cos^2\varphi)^2}{\cos^2\varphi}\right], \tag{11b}$$

where θ_b is boundary layer potential temperature (replaced in moist atmospheres by θ_{eb}, the subcloud equivalent potential temperature), θ_{ba} is the value of θ_b at φ_a, T_s is the surface temperature, T_t is the temperature at the tropopause, and $T_s - T_t$ has been assumed constant.[9]

Blue curves in Figures 2(a) and 3(a) show these for $\varphi_a = 0°$ and $\varphi_a = 21.2°$. In both cases, φ_a corresponds to a local thermal maximum, since then $u = 0$ throughout the column as assumed in deriving u_{amc} and, in turn, (11a) and (11b) (see also Privé and Plumb 2007b). But importantly, it does not follow that $\varphi_a = \varphi_m$, c.f. the previous discussion.

(11a) and (11b) are largely similar, and three key differences between them — gH vs. $c_p(T_s - T_t)$, whether or not there is an exponential operator, and $\hat{\theta}$ and θ_0 vs. θ_b and θ_{bm} — are readily understood. First, CQE in a dry atmosphere implies that dry convection is sufficiently frequent and vigorous as to maintain dry adiabatic stratification, $\Gamma_d = g/c_p$, where Γ_d is the dry adiabatic lapse rate, g is the gravitational constant, and c_p is the atmosphere's heat capacity at constant pressure. Therefore, $T_t = T_s - \Gamma_d H = T_s - gH/c_p$, where H is the tropospheric depth, such that $c_p(T_s - T_t) = gH$. This also applies in the corresponding $f\eta < 0$ expressions, namely (5c) for the Boussinesq case and Eq. 10 of E95 for the CQE case. Second, the exponential operator in (11b) arises from expressing the thermodynamic equation in terms of entropy, $c_p \ln\theta$, rather than θ itself (moist entropy and equivalent potential temperature in a moist atmosphere) (see e.g. Ch. 1 of Vallis 2017). A first-order Taylor expansion of (11b) yields

$$\frac{\theta_b(\varphi) - \theta_{ba}}{\theta_{ba}} \approx -\frac{\Omega^2 a^2}{2c_p(T_s - T_t)} \frac{(\cos^2\varphi_a - \cos^2\varphi)^2}{\cos^2\varphi}, \tag{11c}$$

[8] Fang and Tung (1996) derive an analytic "viscous correction" to their otherwise inviscid solution that accounts for this, which acts to smear out the otherwise step changes in temperature and zonal velocity at their cell edges (see their Figure 4).

[9] Note that Eq. 11 of E95 inadvertently omits the 1/2 factor within the exponential.

Third, under CQE, convection out of the boundary layer sets the adiabatic stratification, such that the entropy value throughout the free troposphere is the local boundary layer entropy (subcloud saturation moist entropy in a moist model). Meanwhile, the reference potential temperature θ_0 in (11a) arises from the expression of hydrostatic balance in the Boussinesq model: $\partial_z \Phi = -(g/\theta_0)\theta$, where $\Phi = gz$ is geopotential. Combining these three arguments, (11c) is essentially the same as (11a): the Boussinesq $\hat{\theta}_{\rm amc}$ amounts to a linearization about $\varphi_{\rm a}$ of its dry CQE counterpart.

The near-equivalence of (11a) and (11b) is demonstrated in Figure 5, which shows (11a) and (11b) over one hemisphere with forcing maxima of 0, 20, 40, 60, and 80°N, assuming $\theta_{\rm ba} = 350$ K and $T_{\rm s} - T_{\rm t} = 100$ K in the E95 solution, and with the LH88 parameters $H = 13$ km and $\theta_0 = 300$ K chosen subjectively to minimize the difference between the two models.[10] Both versions are mirror-symmetric about the equator, with $\sim\cos^4\varphi$ dependence at the equator for $\varphi_{\rm a} = 0°$, thereby preventing equatorial westerlies as previously discussed. The Boussinesq solutions have the undesirable feature of passing through absolute zero, but the CQE cases likewise lose their physical meaningfulness as surface temperatures drop for a given $T_{\rm t}$, certainly once $\theta_{\rm b} \sim T_{\rm t}$. Notice that in all $\varphi_{\rm a} \neq 0$ cases $\hat{\theta}_{\rm rce}$ has negative curvature over most of the span from the equator to $\varphi_{\rm a}$, leveling off just equatorward of $\varphi_{\rm a}$.

Figure 6 shows (11b) for the limiting cases of $\varphi_{\rm a} = 0°$ and $\varphi_{\rm a} = 90°$ and for rotation rates ranging from 4× to $1/16 \times \Omega_{\rm E}$, where $\Omega_{\rm E}$ is Earth's rotation rate. As Ω decreases, meridional gradients in $\hat{\theta}_{\rm amc}$ decrease, varying over the globe by a few Kelvin or less for $\Omega \leq 1/8 \times \Omega_{\rm E}$. This is broadly consistent with the simulations of Faulk et al. (2017), in which an otherwise Earth-like aquaplanet exhibits nearly pole-to-pole ITCZ migrations over its annual cycle in cases with $\Omega \leq 1/8 \times \Omega_{\rm E}$.

3) DIRECT $u_{\rm rce}$ VS. $u_{\rm amc}$ COMPARISON

The AMC model is made globally complete by stipulating that the solution jumps at the Hadley circulation outer edges from the AMC solution to the RCE profile. This is shown in the dotted purple curves of Figures 2 and 3 (with the latitudes of the cell edges determined using the equal-area model as described below). For $\varphi_{\rm m} = 0°$ and assuming no double ITCZ emerges, then $\varphi_{\rm a} = 0°$ as well, so that the resulting AMC cells homogenize the equatorial planetary angular momentum value over their expanse.

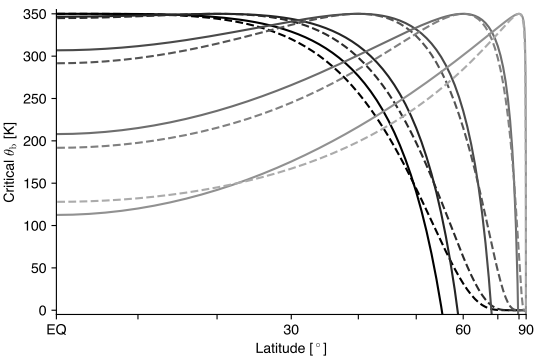

FIG. 5. (Solid curves) Boussinesq $\hat{\theta}_{\rm amc}$ fields given by (11a) and (dashed curves) CQE $\theta_{\rm b}$ fields for an AMC Hadley cell given by (11b). Pairs of curves with the same gray shading are the solutions for a given $\varphi_{\rm a}$, ranging from 0° to 80° by 20° increments. In all cases the potential temperature value at the maximum is set to 350 K. For the CQE profiles, the difference between the surface and tropopause temperatures, $T_{\rm s} - T_{\rm t}$, is taken as a constant 100 K. The free parameters of the LH88 profiles were then chosen subjectively to minimize the differences between the LH88 and E95 solutions. In particular, the given tropospheric depth is 13 km, and the reference potential temperature is 300 K.

The jump from $u_{\rm amc}$ to $u_{\rm rce}$ at the cell outer edges must occur where $u_{\rm rce} \leq u_{\rm amc}$: a cell terminating where $u_{\rm rce} > u_{\rm amc}$ would yield an isolated local maximum in M at the cell edge, thereby still violating Hide's constraint — i.e. if in Fig. 2(c) or Fig. 3(c) the jump from the AMC to RCE curves was upward. It follows that the span between the two $u_{\rm rce} = u_{\rm amc}$ points farthest from each other constitutes a lower bound on the circulation extent (HH80).

This suggests that a cross-equatorial Hadley cell must always extend at least as far into the winter hemisphere as it does into the summer hemisphere. By (10), $u_{\rm amc} = 0$ at both $\varphi_{\rm a}$ and $-\varphi_{\rm a}$. Provided $\hat{\theta}_{\rm rce}$ decreases monotonically from the equator to the winter pole (however modestly), then $u_{\rm rce} > 0$ throughout the winter hemisphere. It follows that $u_{\rm rce} > u_{\rm amc}$ from the equator to some latitude poleward of $-\varphi_{\rm a}$. Even if the meridional slope of $\hat{\theta}_{\rm rce}$ vanishes in the winter hemisphere (as it does in the simulations we present in Section 4), then $u_{\rm rce} = 0$, which is still more westerly than the AMC easterlies spanning from the equator to $-\varphi_{\rm a}$.[11]

We can be more precise for the HH80 case and, to a lesser degree, the LH88 case. For HH80, equating (7b) and (10) with $\varphi_{\rm a} = 0$ yields $\varphi^* = \arccos((1 + 2R)^{-1/4})$,

[10] How well the E95 and LH88 solutions align is sensitive to the values of their free parameters. As the assumed tropospheric depth is increased or reference potential temperature decreased in the LH88 solution, the profiles decrease more rapidly with latitude moving away from the forcing maximum. For example, if the tropospheric depth is set to 10 km, the equatorial potential temperature of the $\varphi_{\rm a}$ =80° solution reduces by ~70 K (not shown).

[11] A seeming counterexample to this argument are the cells in the weakly forced regime of PH92 (see their Fig. 2 and corresponding discussion), which are essentially confined to the summer hemisphere. However, as PH92 note, the forcing in these simulations is sufficiently small given the small but finite viscosity that the cells are still in the viscous limit. As such, the free tropospheric zonal wind field is not angular momentum conserving, and the argument does not apply. The cells in the strongly forced regime do extend comparably into either hemisphere (their Fig. 5).

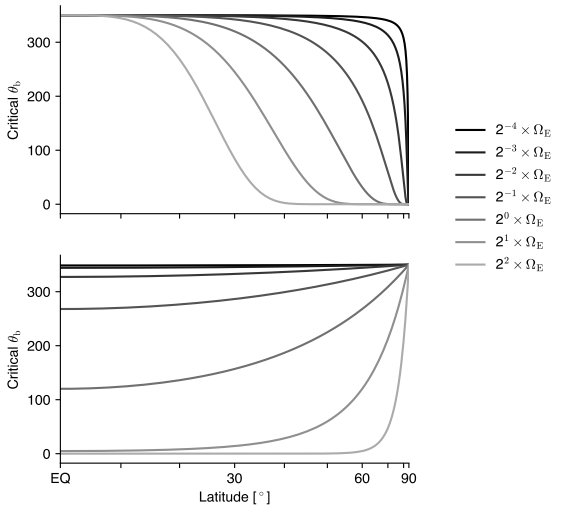

FIG. 6. Boundary layer potential temperature profiles from E95 (or, for a moist atmosphere, subcloud equivalent potential temperature profiles) yielding AMC wind at the tropopause, assuming a fixed temperature difference between the tropopause and surface, as a function of planetary rotation rate for forcing that maximizes (top) at the equator or (bottom) at the north pole. The rotation rate relative to Earth's for each curve is given by the legend; rotation rate could be replaced with planetary rate and the solutions would be identical. In all cases the θ_b value at the maximum is set to 350 K, and the difference between the surface and tropopause temperatures, $T_s - T_t$, is taken as a constant 100 K. Note that these solutions are mirror symmetric about the equator.

where φ^* is the cell edge, or equivalently $\varphi^* = \arctan([(1+2R)^{1/2}-1]^{1/2})$ as expressed by HH80. For LH88, the choice of φ_a is much less obvious, c.f. the previous discussion. If it is the case that $\varphi_a \approx \varphi_m$, then equating (7a) and (10) yields

$$2R\left(1-\frac{\sin\varphi_m}{\sin\varphi^*}\right)=\frac{\cos^4\varphi_m}{\cos^4\varphi^*}-1.$$

$\varphi=\varphi_m$ is always a solution (where $u_{rce}=u_{amc}=0$), but the remaining solutions are not attainable analytically.

c. Equal-area solutions

Advancing from lower bounds on the overall circulation's poleward edges to precise expressions for φ_a and each cell's poleward edge is possible via the equal-area model introduced by HH80 for $\varphi_a = 0$ and extended to $\varphi_a \neq 0$ by LH88. Because (11a) is expressed in terms of its own value at φ_a, closing the system requires solving for this value $\hat{\theta}_{amc}(\varphi{=}\varphi_a)$ in addition to the cell edge locations. Closure can be provided by a pair of assumptions involving the thermodynamic structure of the cells. First, the column-averaged potential temperature switches continuously from $\hat{\theta}_{amc}$ to $\hat{\theta}_{rce}$ at the circulation's poleward edge; second, flow within each cell conserves energy. If $\hat{\theta}_{rce}$ is symmetric about the equator and $\varphi_a = 0$, the two cells are mirror symmetric, yielding two equations to solve for the two unknowns:

$$\hat{\theta}(\varphi_H)=\hat{\theta}_{rce}(\varphi_H), \tag{12a}$$

$$0=\int_0^{\varphi_H}(\hat{\theta}-\hat{\theta}_{rce})\cos\varphi\,d\varphi, \tag{12b}$$

where φ_H is the latitude of one of the cell's poleward edge. If $\varphi_a \neq 0$, the model becomes four equations in four unknowns (the winter cell poleward edge, φ_a itself, the potential temperature at φ_a, and the summer cell poleward edge; see Equations 8-11 of LH88).

Purple dotted curves in Figure 2 show the equal-area solution for the HH80 case, i.e. with $\hat{\theta}_{rce}$ given by (7b), and with $\theta_0 = 300$ K, $H = 10$ km, and $\Delta_h = 1/3$, such that $R \approx 0.15$. Also overlaid are the spans of all the extent metrics — from the equal area solution (with dots denoting the three cell edges), $u_{rce} = u_{amc}$ with u_{amc} computed using the value of φ_a from the equal-area model, and $M > \Omega a^2$ (recall that neither $f\eta < 0$ or $M < 0$ occur at any latitude). In this case, the $M > \Omega a^2$ and $u_{rce} > u_{amc}$ criteria are identical, since $\varphi_a = 0°$ and thus the M value being homogenized by u_{amc} is $M = \Omega a^2$.

In the small angle limit, the HH80 equal-area solution terminates at $\varphi_H = (5R/3)^{1/2}$, a factor of $(5/3)^{1/2}$ poleward of where $u_{rce} = u_{amc}$. Without the small angle assumption, an analytical solution is no longer attainable, but the resulting expression (Eq. 17 of HH80) is readily solvable numerically and always yields a cell terminating poleward of the $u_{rce} = u_{amc}$ line. This is demonstrated in Figure 7, which shows $u_{rce} = u_{amc}$ and the equal-area cell edge for $0.001 \leq R \leq 10$ both with and without the small-angle approximation. As the thermal Rossby number increases beyond the range shown, the equal-area edge approaches the pole for $R \sim 20$, at which value the $u_{rce} = u_{amc}$ marker is $\sim 70°$.

Figure 3 includes the equal area solutions for the LH88 case, i.e. with $\hat{\theta}_{rce}$ given by (7a) with $\varphi_m = 6°$. Because $\varphi_m \neq 0$, the value of M depends on the solution for φ_a and u_{rce} is no longer symmetric about the equator; as such the $u_{amc} = u_{rce}$ and $M > \Omega a^2$ conditions are no longer identical. It can be seen that the equal area φ_a prediction is appreciably *poleward* of φ_m.

As φ_m is moved farther poleward with other parameter values fixed, the winter cell grows and the summer cell shrinks. In fact, for large φ_m, the equal-area solutions are not mathematically unique: depending on the initial guess provided to the numerical solver, either a two-celled or one-celled solution (i.e. φ_a and the summer cell poleward edge are identical) can emerge. Often in these cases the one-celled solution is physically inconsistent, with $u_{rce} > u_{amc}$ at the summer edge (not shown). But for sufficiently large φ_m, the one cell solution is physically valid, with φ_a

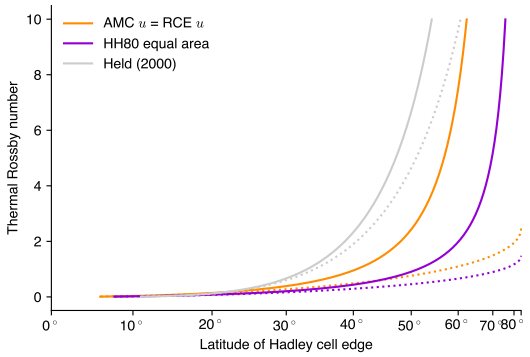

FIG. 7. Edge metrics for the HH80 forcing from (red curves) the $u_{\rm rce} = u_{\rm amc}$ condition and (blue curves) the equal-area model. Also included (gray curves) is the Held (2000) metric based on the two-layer model criterion for the onset of baroclinic instability. For each, solutions are shown both (dotted curves) in the small-angle limit and (solid curves) in the more general case.

occurring where $u_{\rm amc} = u_{\rm rce}$ and hence where $\hat{\theta}_{\rm rce}$ and $\hat{\theta}_{\rm amc}$ lie tangent to one another.[12]

Figures 8 and 9 repeat Figures 2 and 3 but with $\Omega = 1/4 \times \Omega_{\rm E}$, yielding $R \approx 2.4$. The features are largely similar to their faster-rotating counterparts, just meridionally expanded: for the $\varphi_{\rm m} = 0$ case, the cell poleward edges now occur at $\pm 62.4°$. For the $\varphi_{\rm m} = 6°$ case, $\varphi_{\rm a}$ is displaced only slightly poleward compared to the $1 \times \Omega_{\rm E}$ case, 21.2 vs. 23.1°, but the poleward edges expand from -40.5 and 30.7° to -69.1 and 62.0°. For either R value, the $u_{\rm rce} = u_{\rm amc}$ lower bound is within ~15° of the adjacent equal-area edge and is a more useful approximation than the combined spans of $M > \Omega a^2$, $M < 0$, and $f\eta < 0$; it also extends as far into the winter as the summer hemisphere.

We conclude this section by noting that in non-axisymmetric atmospheres eddy processes likely lead to the cell being truncated equatorward of both the equal-area and supercritical edges. Figure 7 also includes the solutions from Held (2000, Ch. 6) relating the cell edge to the onset of baroclinic instability in a simple two-layer model:

$$R\Delta_{\rm v} = \frac{\sin^4 \varphi_{\rm H}}{\cos^2 \varphi_{\rm H}}, \tag{13}$$

where $\Delta_{\rm v} = 1/8$ is the RCE vertical fractional potential temperature change. In the small-angle limit this reduces to $\varphi_{\rm H} = (R\Delta_{\rm v})^{1/4}$. This yields a Hadley cell edge that is well equatorward of one or both of the axisymmetric-based predictors for all thermal Rossby numbers. However, its relevance becomes questionable at thermal Rossby numbers for which the Rossby radius of deformation, L_R, approaches the planetary scale, where $L_R = NH/f$ and $N \approx \sqrt{(g/\theta_0)\partial_z\theta}$ is the Brunt-Väisälä frequency. Using $\varphi = 30°$, $\theta_0 = 300$ K, $\partial_z\theta = 4$ K km^{-1}, and taking variations in R and L_R to occur through variations in Ω, $L_r \approx a$ at $R \approx 2.5$. A follow-up study will explore the role of eddies in more detail, including comparison

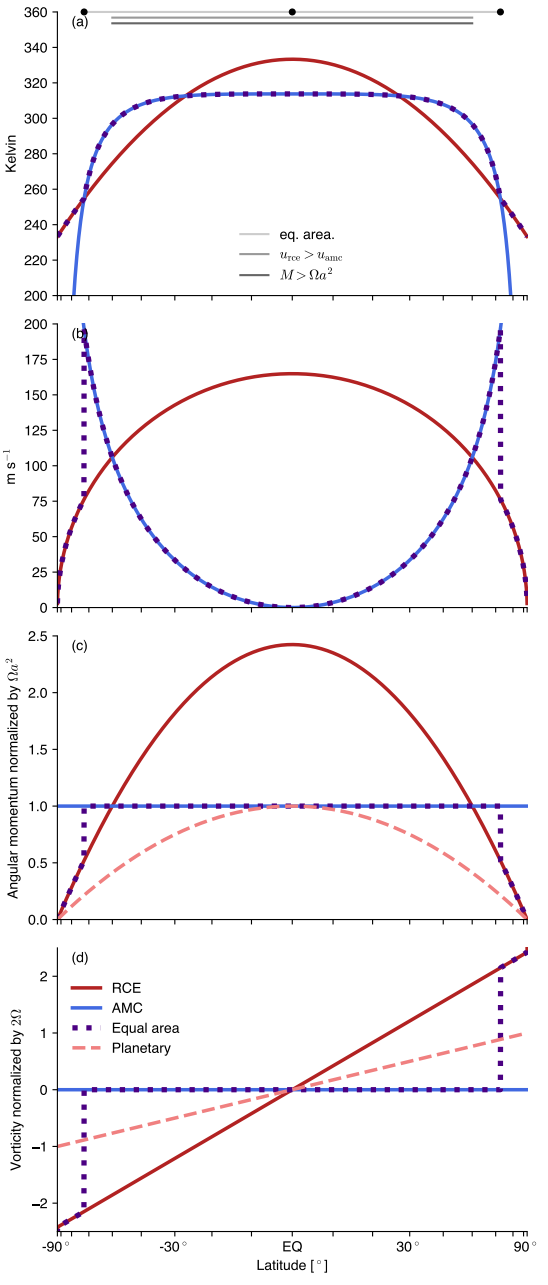

FIG. 8. Same as Fig. 2, but with $\Omega = \Omega_{\rm E} \times 1/4$, and thus $R \approx 2.4$. Note different vertical axis spans than in Fig. 2.

[12] As $\varphi_{\rm m}$ moves poleward, the lowest values of $\hat{\theta}_{\rm rce}$, which occur near the winter pole, decrease, becoming negative for $\varphi_{\rm m} \gtrsim 55°$ at Earth's rotation rate. Interestingly, in these physically impossible cases, the equal area model still yields a mathematically valid two-cell solution, but one in which angular momentum jumps from a lower to a higher M value at its summer poleward edge (not shown).

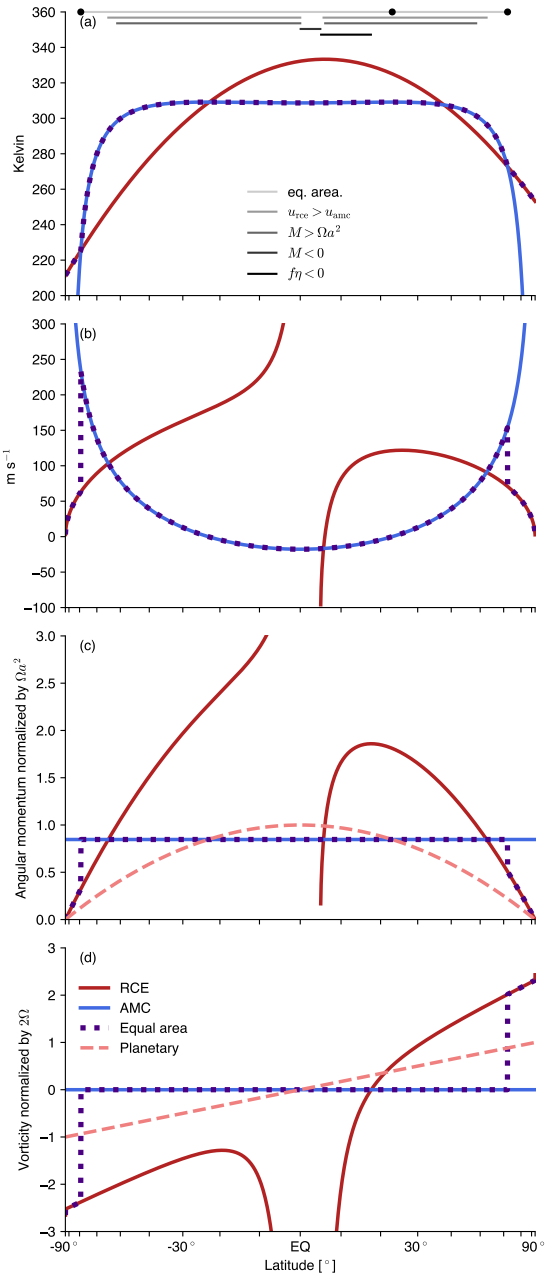

FIG. 9. Same as Fig. 3, but with $\Omega = \Omega_E \times 1/4$, and thus $R \approx 2.4$. Note different vertical axis spans than in Fig. 3.

of the Held (2000) argument with more physically realistic approaches (c.f. Korty and Schneider 2008; Levine and Schneider 2015).

4. Results from sub- and supercritically forced simulations

Provided one of the onset criteria of Section 2 is met, it should be possible to generate Hadley cells of arbitrary latitudinal extent via radiative forcing that satisfies some combination of the extent conditions of Section 3 over the cell's full range. This section assesses this claim through simulations in an idealized GCM.

a. Description of the idealized dry GCM

We use the dry idealized GCM introduced by Schneider (2004), which solves the primitive equations on the sphere with no topography using a spectral dynamical core. All parameters take Earth-like values except as otherwise noted. The simulations are axisymmetric by way of exactly axisymmetric initial conditions and boundary conditions.

There are three dissipative processes: ∇^8 hyperdiffusion to represent subgrid-scale dissipation, quadratic damping of winds within the planetary boundary layer to represent surface drag, and vertical diffusion in the free atmosphere to suppress symmetric instabilities that otherwise cause the model to crash. The quadratic drag formulation is $\partial_t \mathbf{u} = \cdots - k(\sigma)\,|\mathbf{u}|\,\mathbf{u}$, where $\mathbf{u} = (u, v)$, is the horizontal wind vector, $|\mathbf{u}| = (u^2 + v^2)^{1/2}$ is the horizontal wind speed, and $k(\sigma)$ is the drag coefficient, which takes its maximal value at the surface and decreases linearly in the model's vertical sigma coordinate ($\sigma \equiv p/p_s$, where p_s is the spatiotemporally varying surface pressure) to a value of zero at $\sigma_{b,top}$, the prescribed boundary layer top. For the planetary boundary layer, we raise the top from its default of 0.85 to 0.7 and double the drag coefficient from its default value of 5×10^{-6} m^{-1} in order to suppress a pronounced "equatorial jump" in the Hadley cells (Pauluis 2004), although such jumping remains appreciable despite these and additional measures described below intended to prevent it. Free atmospheric viscosity is formulated as standard as vertical diffusion, such that $\partial_t \mathbf{u} = \cdots + \partial_z(\nu \partial_z \mathbf{u})$ for zonal and meridional momentum and analogously for temperature with Prandtl number unity. This is turned on only at model levels above a fixed height of 2500 m, a slightly different boundary layer top criterion than the fixed sigma level used by the boundary layer drag scheme.[13]

[13] Rather than the commonly-used uniform ν (e.g. HH80, LH88, PH92, Bordoni and Schneider 2010), the model uses a mixing length formulation:

$$\nu = l_{mix}^2 \left(1 - \frac{\mathrm{Ri}}{\mathrm{Ri}_{crit}}\right)^2 \frac{|\Delta \mathbf{u}|}{\Delta z},$$

where l_{mix} is the mixing length (a global constant), Ri is the bulk Richardson number, $\mathrm{Ri}_{crit} \equiv 0.25$ is a critical Richardson number above which free atmospheric diffusion does not occur, Δ denotes differences between adjacent model levels, and $|\Delta \mathbf{u}| = ((\Delta u)^2 + (\Delta v)^2)^{1/2}$. The bulk Richardson number is defined conventionally, $\mathrm{Ri} = g\Delta\theta\Delta z/(\theta|\Delta \mathbf{u}|^2)$. Under this formulation, the diffusivity increases with the vertical shear of the horizontal wind speed and decreases with the static stability $\partial_z \theta$. We have experimented with a range of mixing length values in a subset of the simulations in order to find the lowest value in which the model integration runs successfully; that value is 15 m in all simulations except the most strongly forced simulation at Earth's rotation rate, which required a value of 30 m.

Convective adjustment relaxes temperatures in statically unstable columns toward $\gamma\Gamma_d$ over a globally uniform 4 day timescale. Other studies have set $\gamma = 0.7$ to mimic the stabilizing effects of moisture (e.g. Schneider and Bordoni 2008), but we set it to unity given our focus on dry atmospheres. Radiative transfer is approximated by Newtonian cooling, wherein temperatures are relaxed toward a prescribed field (described in the next subsection) over a timescale that is 50 days throughout the free troposphere and decreases linearly in σ from that value at the PBL top to 7 days at the surface.

b. Imposed RCE temperature profiles

The GCM uses the full primitive equations without the Boussinesq assumptions, and so we use the CQE framework for specifying the equilibrium temperature fields being relaxed toward. Specifically, the equilibrium temperature fields at the lowest model level (which we refer to as the surface values) are based on (11b), modified as described below, with a dry adiabatic lapse rate from the surface to a specified tropopause temperature. The atmosphere is isothermal from the tropopause upwards. The dry adiabatic stratification, along with the dry adiabatic convective adjustment, ensures little distinction between the imposed equilibrium temperatures and a true RCE solution.[14]

Under purely dry adiabatic stratification as in the RCE state, the cells would transport no heat as they overturn; the implication is that the circulation generates some positive static stability, since the simulated Hadley cells are thermally direct in all cases. Caballero et al. (2008) cites penetration of the cell into the positively stratified stratosphere and the horizontal homogenization of the upper branch θ equal to the surface θ value within the ascending branch as mechanisms for generating this positive stability.

Starting from (11b), we insert a multiplicative factor, α, into the exponential, with $\alpha = 2.0$ to generate cells that extend to the vicinity of φ_m and $\alpha = 0.5$ to generate cells that terminate well equatorward thereof. At 10° past the forcing maximum φ_m, the temperature uniformly takes the value at 10°, since otherwise except for $\varphi_m = 90°$ the profile would drop toward absolute zero. To generate a cross-equatorial circulation, at $\varphi = 10°$ in the summer hemisphere (always chosen to be the NH) we switch from the original profile to its tangent at that point, following this linear change in latitude across the equator to $\varphi = 10°$ in the winter hemisphere. Temperature is constant from this point to the winter pole.

c. Simulations performed

We perform a two-dimensional parameter sweep of the planetary rotation rate ($\Omega = 1\times$, $1/2\times$, and $1/4\times\Omega_E$, where Ω_E is Earth's rotation rate) and the latitude of the imposed forcing maximum (φ_m =23.5°, 45°, and 90°). For each (Ω, φ_m) pair, we perform two simulations, one with $\alpha = 0.5$ and one with $\alpha = 2.0$. Table 1 lists the forcing parameters for each simulation, and Figure 10 shows the imposed equilibrium surface temperature profiles in each simulation, as well as the spans where the $f\eta < 0$, $M < 0$, and $M > \Omega a^2$ conditions for cell extent are met (η, u_{rce}, and M fields themselves are not shown). The linear increase in temperature spanning the equator in all cases ensures $M > \Omega a^2$ on the winter-side of the equator and $M < 0$ on the summer-side. In the $\alpha = 2.0$, $\varphi_m = 90°$ cases, this region extends all the way to the pole. In all other cases, poleward of the $M < 0$ region there exists a finite region where $f\eta < 0$ in the summer hemisphere. The combined range of these extent conditions spans ~10°S-10°N in the $\alpha = 0.5$ cases (i.e. those latitudes with the linear temperature profile), compared to φ_m or somewhat poleward thereof in the $\alpha = 2.0$ cases.

Parameter values were chosen on an ad hoc basis for each (Ω, φ_m) pair in order (1) to generate supercritical forcing from the equator to φ_m in the $\alpha = 2.0$ case with the minimal meridional temperature variation possible, and (2) with surface temperatures near the equator ~300 K in all cases (so that the tropospheric depth is similar across simulations, at least away from φ_m). For forcing maxima well removed from the Tropics at Earth's rotation rate, it is difficult to generate $f\eta < 0$ near φ_m while keeping a realistic tropopause depth. For this reason, the tropopause is set to 100 K in our forcing profiles in some of the $1\times\Omega_E$ cases, in which the forcing surface temperature at the maximum can exceed 500 K. Under dry adiabatic stratification, this yields an effective tropopause height of ~40 km. Stated another way, if we require that the tropospheric depth remains roughly Earth-like, we are unable to violate Hide's constraint near φ_m at Earth's rotation rate or faster for high-latitude φ_m.

Table 1 also lists diagnosed values of Δ_h, computed as the global maximum minus the global minimum of the surface forcing temperature divided by its global mean, and the corresponding diagnosed value of R. These were diagnosed after the simulations were complete, i.e. they were not tuned for, so it is interesting that the R values are quite similar across Ω values, particularly for $\alpha = 2.0$. For example, $R \sim 1.1$–1.2 in all three $\varphi_m = 90°$, $\alpha = 2.0$ cases.

[14] To confirm this is the case, we have computed RCE solutions for a subset of our cases by repeating them with all advective terms suppressed (not shown): the temperature structure is always almost exactly dry adiabatic from the surface to the tropopause. An alternative approach used by Schneider and Walker (2006) is to have the vertical profile of the relaxation temperatures correspond to radiative equilibrium and to compute RCE solutions explicitly. See also Zalucha et al. (2010) for discussion of the influence of pure radiative equilibrium vs. RCE in nearly inviscid Hadley cell dynamics.

TABLE 1. Forcing parameters of each simulation performed. From left to right: ratio of planetary rotation rate to Earth's rotation rate, where Ω_E is Earth's rotation rate (s^{-1}); latitude of forcing maximum (°); value of α (dimensionless); tropopause temperature (K); difference between surface and tropopause temperatures used in the expression to generate the forcing (K); temperature at the forcing maximum (K); largest fractional temperature variation (dimensionless); and diagnosed thermal Rossby number (dimensionless). Parameter values were chosen so that $\theta_b \sim 300$ K at the equator in all cases.

Ω/Ω_E	φ_m	α	T_t	$T_s - T_t$	T_{max}	Δ_h	R
1	23.5	0.5			303.1	0.01	0.01
		2.0			310.9	0.07	0.05
	45	0.5	100	250	317.5	0.07	0.08
		2.0			371.6	0.27	0.32
	90	0.5		400	344.1	0.15	0.67
		2.0			512.2	0.28	1.25
0.5	23.5	0.5			301.1	6×10^{-3}	0.01
		2.0			304.0	0.03	0.05
	45	0.5			310.5	0.04	0.08
		2.0			342.7	0.17	0.32
	90	0.5		200	321.2	0.07	0.28
		2.0			392.1	0.31	1.16
0.25	23.5	0.5			300.3	2×10^{-3}	0.01
		2.0			301.0	6×10^{-3}	0.05
	45	0.5			302.6	0.01	0.08
		2.0			310.2	0.04	0.32
	90	0.5			310.3	0.04	0.28
		2.0			342.9	0.15	1.13

Also note that these R values are much less than the critical values required for the $f\eta < 0$ condition to be satisfied in the case of LH88 forcing shown in Figure 4. This is because the η distribution depends not just on the total magnitude of meridional temperature variations but on the *shape* of those variations — as discussed previously, the $\hat{\theta}_{rce}$ profiles in Figure 10 "ramp up" with positive curvature moving from the equator toward φ_m, rather than the LH88 cases [Figure 3(a)] in which $\hat{\theta}_{rce}$ has negative curvature.

All simulations are run for 1200 days starting from an isothermal, resting state, with results presented as averages over the last 1000. Though a statistically steady state is achieved throughout the domain generally within 100 days, regular transient symmetric instabilities persist throughout the integration over much of the extent of the Hadley cells (not shown). As one example, in the simulation at Earth's rotation rate with $\varphi_m = 45°$ and $\alpha = 2.0$, equatorward propagating features are prominent from roughly 35°S to 10°S.

d. Results

Figure 11 shows the meridional overturning streamfunctions in each $\alpha = 2.0$ case, and Figure 12 shows the same for the $\alpha = 0.5$ cases, in both with angular momentum contours, the computed Hadley cell edge latitudes, and φ_m overlaid. Particularly as the scale of the Hadley cells grows, ascertaining a clear cell edge can be difficult (Levine and Schneider 2011). We present results based on the commonly used metric of where the meridional overturning streamfunction at the level of its maximum within the cell decreases to 10% of its maximum (Walker and Schneider 2006).

The nonzero forcing gradient spanning the equator necessitates an overturning cell in all cases, and the streamlines of those cells are nearly coincident in the free troposphere with angular momentum contours. Additionally, the cross-equatorial cells extend to nearly the same latitudes in the winter and summer hemispheres, typically somewhat farther into the winter hemisphere, consistent with the heuristic argument made previously regarding the likely extent of the cross-equatorial cell. In all cases, the Hadley circulation comprises a single cross-equatorial cell, with no discernible summer cell. For that reason, the cell edge in the summer hemisphere can be thought of as φ_a.

Also overlaid are the ranges where any of the $M > \Omega a^2$, $M < 0$, and $f\eta < 0$ conditions for cell extent are met, and separately where the $u_{rce} > u_{amc}$ condition is met. The value of φ_a used to compute u_{amc} is diagnosed from the minimum value of angular momentum at the equator: given that value, $M_{eq,min}$, $\varphi_a \approx \arccos(\sqrt{M_{eq,min}/\Omega a^2})$. Roughly speaking, this amounts to finding the angular momentum contour coincident with the circulation's topmost streamline at the equator and tracing it back to the surface in the summer hemisphere. This value (shown as vertical purple line) is generally close to the edge diagnosed from the streamfunction and for the $\alpha = 2.0$ cases is near φ_m also.

This rough coincidence of φ_a and φ_m for $\alpha = 2.0$ lead to a single, nearly pole-to-pole cell in the polar-maximal forcing cases. The biggest offsets of φ_a and the cell edge from φ_m occur in the $\Omega = 1\times\Omega_E$ and $\varphi_m = 90°$, for which the computed cell edge metric sits at ~69°. However, the streamfunction retains its sign all the way to the pole, and the cell is nevertheless global in scale (zonal winds near the equator approach 400 m s^{-1} in the stratosphere in this case; not shown). This is a remarkable contrast to Earth's present-day Hadley circulation, which throughout the annual cycle never extend beyond ~44° in either hemisphere (based on the zero crossings of the overturning streamfunction shown in Figure 4 of Adam et al. 2016).

Notable in the $\alpha = 2.0$ cases are very strong equatorial jumps (Pauluis 2004), with some streamlines bending up out of the boundary layer near ±10° and rising by as much

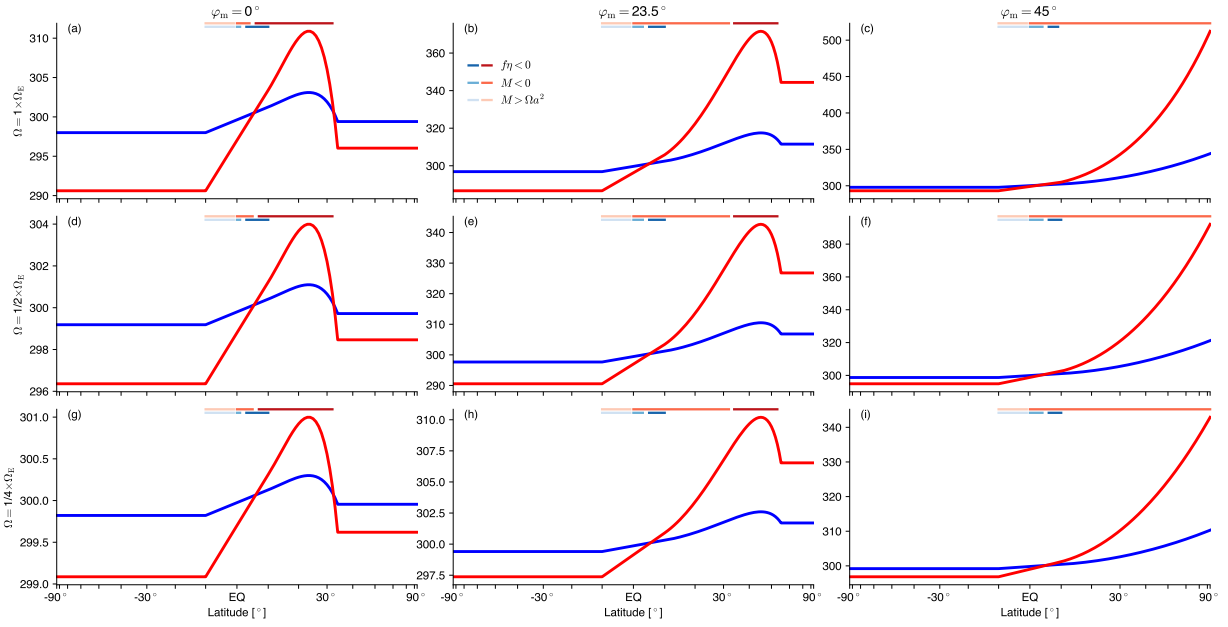

FIG. 10. Equilibrium surface temperature distribution (in Kelvin) that is relaxed toward in each simulation: (left to right) forcing maximum latitude φ_m, (top to bottom) planetary rotation rate, and (thick curves) value of α (blue for $\alpha = 0.5$, red for $\alpha = 2.0$). Horizontal lines at the top of each panel correspond to the extent metrics as indicated in the legend in panel, with blue shades for the $\alpha = 0.5$ case and red shades for $\alpha = 2.0$. Note different vertical axis spans in each panel.

as ~0.4 in σ. The angular momentum contours jump with them. We expect that further tinkering could further suppress this jump — in particular, inserting a multiplicative factor that steepens the otherwise-tangent curve spanning the equator — but it is interesting that away from this region the cells do not seem clearly affected by the jump's presence.

For the $\alpha = 0.5$ cases, the cells typically terminate well equatorward of the forcing maximum — in the most extreme case, with $\Omega = 1/2 \times \Omega_E$ and $\varphi_m = 90°$, φ_a and the cell edge are near 20°. Figure 13 shows θ at $\sigma \approx 0.85$ in all cases. The $\alpha = 0.5$ cell terminates near where $\partial_\varphi \theta_b \approx 0$, but sits just poleward of an inflection point rather than just equatorward of a maximum as suggested by Privé and Plumb (2007a). The flattening of θ_b equatorward of the ascent branch can be interpreted c.f. Schneider and Bordoni (2008) as caused by the southerly flow in the cell's lower branch advecting θ_b up-gradient. This flattens θ_b up to where the meridional flow diminishes, at which point θ_b begins increasing sharply with latitude moving farther poleward. Conversely, with $\alpha = 2.0$ temperatures are minimum near the equator and increase moving into either hemisphere as needed to generate the strong easterlies necessary for the AMC cell.

Though traditionally the equal-area model has been restricted to the forcing profiles of HH80 and LH88, there is no reason it cannot be applied to other forcing profiles. We have attempted to generate equal-area model solutions for the $\hat{\theta}_{rce}$ profiles in our simulations. However, as yet we have been able to get the numerical solver used for the HH80 and LH88 cases used previously to converge to a physically meaningful solution in our cases. But Figure 13 indicates that equal-area-like behavior is indeed occurring (compare the thick dark lines to the corresponding thin pale lines, the latter being θ_{rce}): the dynamically equilibrated $\hat{\theta}$ fields intersect the $\hat{\theta}_{rce}$ fields at low latitudes where the former are flat and the latter are quite steep, in the winter hemisphere from below, and in the summer hemisphere from above, yielding areas between the two curves that, at least by eye, appear to roughly cancel. On the other hand, in all simulations $\varphi_a \leq \varphi_m$, in contradiction to the equal-area prediction.

5. Summary

We have presented theoretical arguments and numerical modeling results pertaining to the emergence and extent of the Hadley cells in steady, dry, axisymmetric, nearly inviscid planetary atmospheres. The theoretical starting point for emergence is Hide's constraint, i.e. that the vertical component of absolute vorticity (η) cannot change sign at any level in which vertical velocity uniformly vanishes. This general form holds even in zonally varying atmospheres, and in the case of axisymmetric atmospheres it prohibits the absolute angular momentum (M from exhibiting global minima (i.e. $M < 0$) or maxima (i.e. $M > \Omega a^2$) away from the surface. At the equator, one

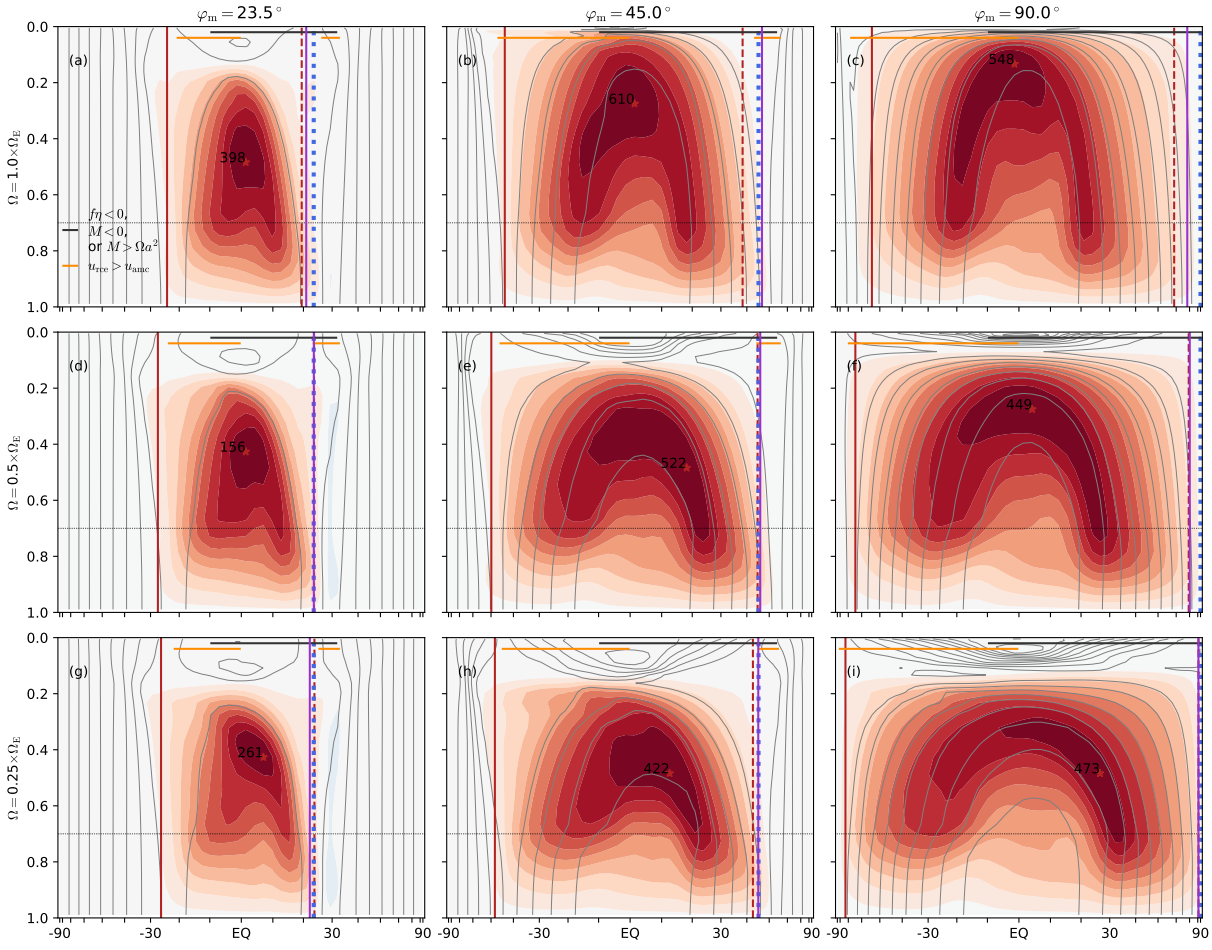

FIG. 11. (Filled contours) meridional overturning streamfunction and (grey contours) absolute angular momentum fields in the simulations with $\alpha = 2.0$ (see text for explanation of the experimental setup) with (left to right) the forcing maximum at 23.5, 45, and 90°N, and (top to bottom) planetary rotation rate 1, 1/2, and 1/4×Earth's rotation rate. In each panel, the contour interval for the streamfunction is 10% of the value at the cell center, labeled by the red star and adjacent text in 10^9 kg s^{-1}, with red shades denoting positive values and blue shades negative values, and the contour interval for the angular momentum is 10% of the planetary angular momentum at the equator. The red vertical lines denote the cross-equatorial Hadley cell's edges in the (solid) winter and (dashed) summer hemisphere, based on where the streamfunction reduces to 10% of its maximum at the same level. The purple solid line denotes the effective φ_a, computed as described in the text. The blue dotted lines correspond to the location of the forcing maximum φ_m. The dotted horizontal line marks the planetary boundary layer top of $\sigma = 0.7$.

or more of these necessarily occur if the RCE potential temperature has a nonzero first meridional derivative or negative second meridional derivative at the equator; the off-equatorial expressions are more involved but are nevertheless easily computed given $\hat{\theta}_{rce}$. The RCE gradient-balanced zonal wind (u_{rce}) value of $-\Omega a \cos\varphi$ below which $M < 0$ is also the lowest value for which u_{rce} has a real-valued solution, an interesting coincidence that we do not fully understand.

A Hadley circulation must span all latitudes that meet one or another of these statements of Hide's constraint, and in some cases strongly forced cases with the forcing maximum (φ_m) off-equator, the combined $M < 0$ and $f\eta < 0$ conditions are met from the equator to near φ_m. In other cases, the minimum cell extent imposed by these ranges is much too small to be useful. The AMC Hadley cell models, which in the Boussinesq and (dry) convective quasi-equilibrium frameworks are closely related, yield cells that must span all latitudes where $u_{rce} = u_{amc}$, but u_{amc} cannot generally be prognosed because φ_a cannot be prognosed. In particular, in cases with a sufficiently modest and/or poleward forcing maximum in the summer hemisphere, the cell can terminate well equatorward thereof. The $u_{rce} = u_{amc}$ lower bound on the circulation extent provides a simple heuristic argument for why cross-equatorial cells typically extend at least as far into the winter hemisphere as into the summer hemisphere in axisymmetric atmospheres.

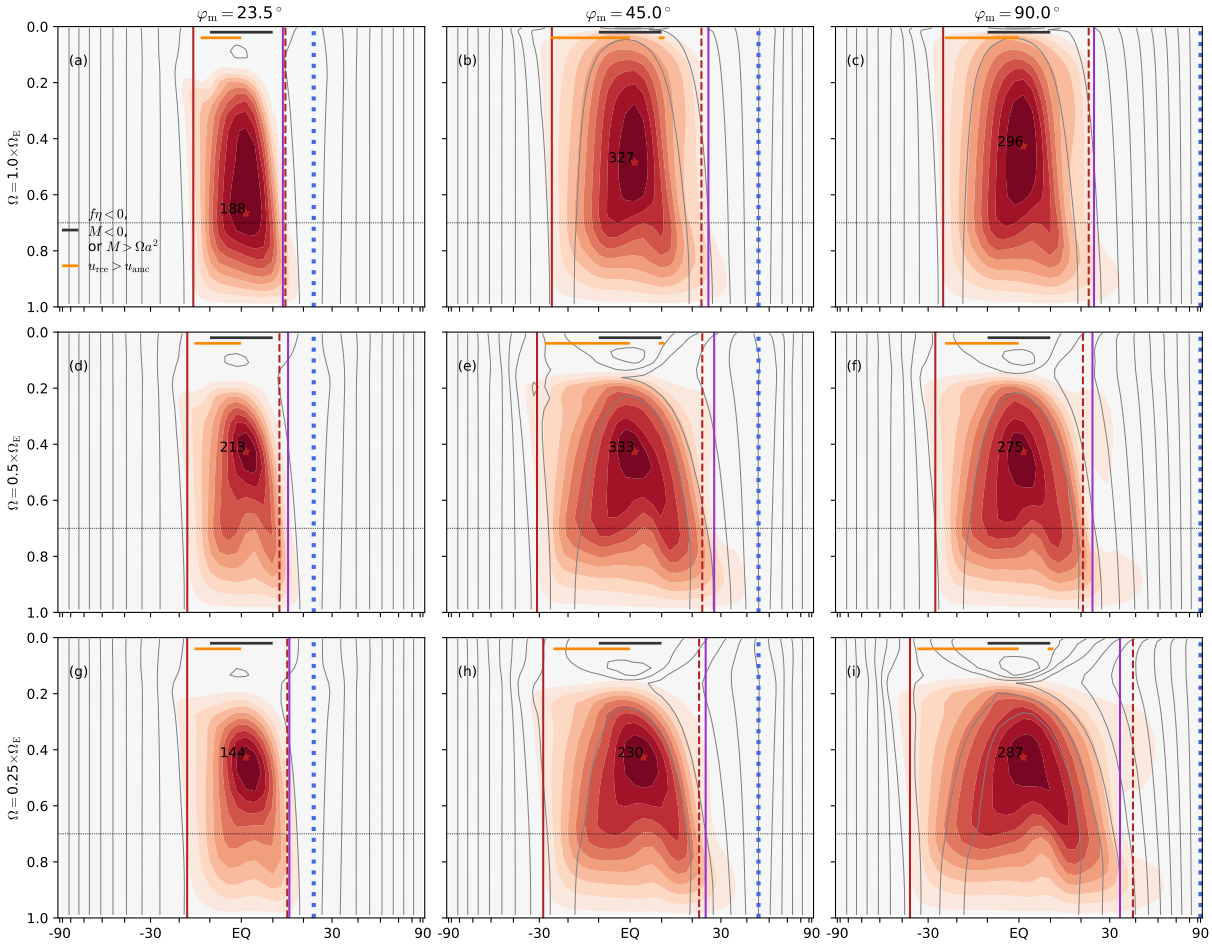

FIG. 12. As in Figure 12, but for the $\alpha = 0.5$ simulations.

In the equal-area models of the Hadley cell based on the assumptions of energy conservation by the cells and continuity of potential temperature at their edges, the predicted cell extent always sits poleward of the range of supercritical forcing and of where $u_{rce} = u_{amc}$, as is necessary for physical self-consistency. These models provide predictions for the edges of each overturning cell, unlike the $u_{amc} = u_{rce}$ condition that sets a lower bound for the extent across all cells. But a drawback is their lack of an analytical solution in all but the HH80 small-angle case.

Simulations in an idealized, dry GCM in which temperatures are relaxed at each timestep toward a specified RCE field that is either subcritical or supercritical in the summer hemisphere up to a specified forcing maximum latitude show the utility of the nearly inviscid arguments: when the forcing is subcritical outside the deep tropics, Hadley cells terminate typically within ~25°of the Equator, in which cases the cell edge sits slightly poleward of an inflection point between flat temperatures equatorward and sharply increasing temperatures poleward. Conversely, when the forcing is supercritical, the cells extend always into the direct vicinity of the forcing maximum, yielding a single, global-scale cell under polar maximal forcing. In all cases, the cells span roughly as far into either hemisphere, in reasonable agreement with the $u_{rce} = u_{amc}$ condition given values of φ_a and u_{amc} fields diagnosed from the simulation output. In addition, φ_a always sits equatorward of φ_m, in contradistinction to the equal-area model.

6. Discussion

We have focused exclusively on the Boussinesq and CQE Hadley cell frameworks, but both effectively amount to single-layer models for the flow at the tropopause. This has led to them being recast as a shallow water equation system, which enables further simplification and theoretical insight. This includes the studies of Adam and Paldor (2009, 2010a,b) for cells with thermal Rossby number ~0.1, who emphasize the roles of vertical momentum advection and of mixing within a finite-width ascent branch. Other useful vertically-reduced models include

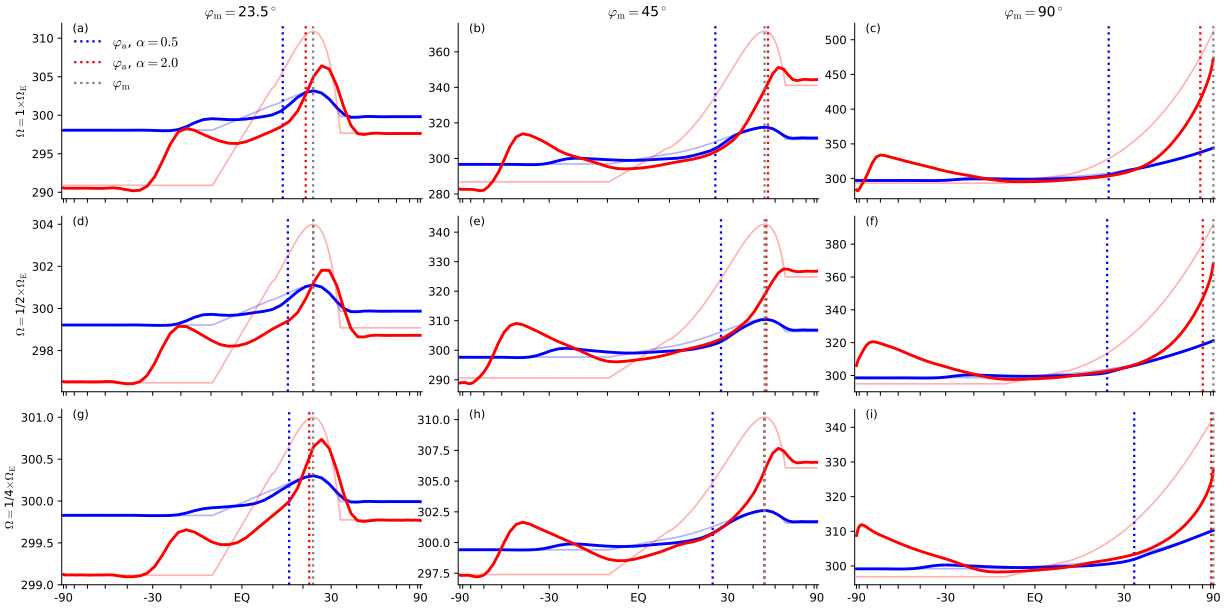

FIG. 13. (Thick solid curves) potential temperature (in K) at the $\sigma \approx 0.85$ level in the (blue) $\alpha = 0.5$ and (red) $\alpha = 2.0$ cases and (thin solid curves) the corresponding forcing values, with panels oriented as in Figure 10. As indicated in the legend in panel (a), vertical dotted lines are the effective ascent latitude for (blue) $\alpha = 0.5$ and (red) $\alpha = 2.0$ and (gray) the forcing maximum latitude. Note different vertical axis spans in each panel.

the weak temperature gradient approach of Polvani and Sobel (2002) and the two-vertical-mode model of Burns et al. (2006).

Given negligible surface wind and meridional temperature gradients that do not change sign in the troposphere, the maximal RCE zonal wind speed at any latitude depends on the local tropopause height. But such meridional variations in the tropopause height are neglected in the existing nearly inviscid, axisymmetric theories. Work is in progress to address this in the CQE model by assuming a fixed tropopause temperature T_t, rather than surface-tropopause temperature difference $T_t - T_s$, and will be presented in a forthcoming manuscript.

One means of directly testing our argument regarding the symmetry in extent of cross-equatorial cells would be simulations in which, rather than flat temperatures in the winter hemisphere, a secondary maximum exists in the winter hemisphere, with its location and magnitude chosen such that the corresponding RCE easterlies on its equatorward side lead to the $u_{rce} = u_{amc}$ transition occurring appreciably equatorward of $-\varphi_a$. If this secondary winter maximum is equatorward of $-\varphi_a$ and sufficiently large (but not as large as the summer maximum; otherwise the interpretation of summer vs. winter hemisphere must be reversed), the easterlies generated on the equatorward side of $-\varphi_a$ could lead to $u_{amc} = u_{rce}$ occurring much closer to the equator. In principle this could lead to a lopsided cell, with the summer hemisphere poleward edge unchanged but the winter hemisphere poleward edge moved appreciably equatorward.

In our simulations, the Hadley cells are all angular momentum conserving in the sense that streamlines and angular momentum contours are nearly coincident in the free troposphere over the circulation's whole expanse. But the true theoretical AMC circulation has a *single* value of M, namely the planetary value at φ_a, whereas the simulated cells feature steadily decreasing M values moving poleward and with it appreciable meridional temperature gradients outside of the tropics. Even if done so empirically, it could be useful to construct a "relaxed" AMC $\hat{\theta}$ profile that gives rise to such behavior, and use it in the place of the true $\hat{\theta}_{amc}$ field in the equal-area model.

These results suggest that Hide's constraint and angular momentum conserving cell theory can be taken to govern the behavior of axisymmetric, nearly inviscid atmospheres both under Earth-like conditions and under more exotic forcings and/or with planetary parameters that give rise to planetary-scale Hadley cells. We view this refinement of the classical dry, Boussinesq, axisymmetric, nearly inviscid theory as a useful step on the community's larger path toward a complete understanding of meridional overturning circulations in eddying, moist atmospheres, both the zonal mean Hadley cells and zonally confined monsoons, in the time mean and as they evolve over the annual cycle or on other timescales.

Acknowledgments. We thank Sean Faulk and Alex Gonzalez for discussions that informed this work and Martin Singh for sharing his valuable insights. S.A.H. was supported by a National Science Foundation (NSF) Atmospheric and Geospace Sciences (AGS) Postdoctoral Research Fellowship, award #1624740. S.B. was supported by NSF award AGS-1462544.

References

Adam, O., T. Bischoff, and T. Schneider, 2016: Seasonal and Interannual Variations of the Energy Flux Equator and ITCZ. Part I: Zonally Averaged ITCZ Position. *J. Climate*, **29 (9)**, 3219–3230, doi:10.1175/JCLI-D-15-0512.1.

Adam, O., and N. Paldor, 2009: Global Circulation in an Axially Symmetric Shallow Water Model Forced by Equinoctial Differential Heating. *J. Atmos. Sci.*, **66 (5)**, 1418–1433, doi:10.1175/2008JAS2685.1.

Adam, O., and N. Paldor, 2010a: Global Circulation in an Axially Symmetric Shallow-Water Model, Forced by Off-Equatorial Differential Heating. *J. Atmos. Sci.*, **67 (4)**, 1275–1286, doi:10.1175/2009JAS3324.1.

Adam, O., and N. Paldor, 2010b: On the role of viscosity in ideal Hadley circulation models. *Geophys. Res. Lett.*, **37 (16)**, L16 801, doi:10.1029/2010GL043745.

Bordoni, S., and T. Schneider, 2008: Monsoons as eddy-mediated regime transitions of the tropical overturning circulation. *Nature Geosci*, **1 (8)**, 515–519, doi:10.1038/ngeo248.

Bordoni, S., and T. Schneider, 2010: Regime Transitions of Steady and Time-Dependent Hadley Circulations: Comparison of Axisymmetric and Eddy-Permitting Simulations. *J. Atmos. Sci.*, **67 (5)**, 1643–1654, doi:10.1175/2009JAS3294.1.

Burns, S. P., A. H. Sobel, and L. M. Polvani, 2006: Asymptotic solutions of the axisymmetric moist Hadley circulation in a model with two vertical modes. *Theor. Comput. Fluid Dyn.*, **20 (5-6)**, 443–467, doi:10.1007/s00162-006-0024-z.

Caballero, R., and M. Huber, 2010: Spontaneous transition to superrotation in warm climates simulated by CAM3: WARM CLIMATE SUPERROTATION. *Geophysical Research Letters*, **37 (11)**, n/a–n/a, doi:10.1029/2010GL043468.

Caballero, R., R. T. Pierrehumbert, and J. L. Mitchell, 2008: Axisymmetric, nearly inviscid circulations in non-condensing radiative-convective atmospheres. *Q.J.R. Meteorol. Soc.*, **134 (634)**, 1269–1285, doi:10.1002/qj.271.

Emanuel, K. A., 1986: An Air-Sea Interaction Theory for Tropical Cyclones. Part I: Steady-State Maintenance. *J. Atmos. Sci.*, **43 (6)**, 585–605, doi:10.1175/1520-0469(1986)043⟨0585:AASITF⟩2.0.CO;2.

Emanuel, K. A., 1995: On Thermally Direct Circulations in Moist Atmospheres. *J. Atmos. Sci.*, **52 (9)**, 1529–1534, doi:10.1175/1520-0469(1995)052⟨1529:OTDCIM⟩2.0.CO;2.

Emanuel, K. A., J. David Neelin, and C. S. Bretherton, 1994: On large-scale circulations in convecting atmospheres. *Q.J.R. Meteorol. Soc.*, **120 (519)**, 1111–1143, doi:10.1002/qj.49712051902.

Fang, M., and K. K. Tung, 1994: Solution to the Charney Problem of Viscous Symmetric Circulation. *Journal of the Atmospheric Sciences*, **51 (10)**, 1261–1272, doi:10.1175/1520-0469(1994)051⟨1261:STTCPO⟩2.0.CO;2.

Fang, M., and K. K. Tung, 1996: A Simple Model of Nonlinear Hadley Circulation with an ITCZ: Analytic and Numerical Solutions. *J. Atmos. Sci.*, **53 (9)**, 1241–1261, doi:10.1175/1520-0469(1996)053⟨1241:ASMONH⟩2.0.CO;2.

Fang, M., and K. K. Tung, 1999: Time-Dependent Nonlinear Hadley Circulation. *J. Atmos. Sci.*, **56 (12)**, 1797–1807, doi:10.1175/1520-0469(1999)056⟨1797:TDNHC⟩2.0.CO;2.

Faulk, S., J. Mitchell, and S. Bordoni, 2017: Effects of Rotation Rate and Seasonal Forcing on the ITCZ Extent in Planetary Atmospheres. *J. Atmos. Sci.*, **74 (3)**, 665–678, doi:10.1175/JAS-D-16-0014.1.

Gierasch, P. J., 1975: Meridional Circulation and the Maintenance of the Venus Atmospheric Rotation. *J. Atmos. Sci.*, **32 (6)**, 1038–1044, doi:10.1175/1520-0469(1975)032⟨1038:MCATMO⟩2.0.CO;2.

Haberle, R. M., J. B. Pollack, J. R. Barnes, R. W. Zurek, C. B. Leovy, J. R. Murphy, H. Lee, and J. Schaeffer, 1993: Mars atmospheric dynamics as simulated by the NASA Ames General Circulation Model: 1. The zonal-mean circulation. *Journal of Geophysical Research: Planets*, **98 (E2)**, 3093–3123, doi:10.1029/92JE02946.

Held, I. M., 2000: The General Circulation of the Atmosphere. *The General Circulation of the Atmosphere: 2000 Program in Geophysical Fluid Dynamics*, No. WHOI-2001-03, Woods Hole Oceanog. Inst. Tech. Rept., Woods Hole Oceanographic Institution, 1–54.

Held, I. M., 2005: The Gap between Simulation and Understanding in Climate Modeling. *Bull. Amer. Meteor. Soc.*, **86 (11)**, 1609–1614, doi:10.1175/BAMS-86-11-1609.

Held, I. M., and B. J. Hoskins, 1985: Large-scale eddies and the general circulation of the troposphere. *Advances in Geophysics*, Vol. 28A, Academic Press, 3–31.

Held, I. M., and A. Y. Hou, 1980: Nonlinear Axially Symmetric Circulations in a Nearly Inviscid Atmosphere. *J. Atmos. Sci.*, **37 (3)**, 515–533, doi:10.1175/1520-0469(1980)037⟨0515:NASCIA⟩2.0.CO;2.

Held, I. M., and M. J. Suarez, 1994: A Proposal for the Intercomparison of the Dynamical Cores of Atmospheric General Circulation Models. *Bull. Amer. Meteor. Soc.*, **75 (10)**, 1825–1830, doi:10.1175/1520-0477(1994)075⟨1825:APFTIO⟩2.0.CO;2.

Hide, R., 1969: Dynamics of the Atmospheres of the Major Planets with an Appendix on the Viscous Boundary Layer at the Rigid Bounding Surface of an Electrically-Conducting Rotating Fluid in the Presence of a Magnetic Field. *J. Atmos. Sci.*, **26 (5)**, 841–853, doi:10.1175/1520-0469(1969)026⟨0841:DOTAOT⟩2.0.CO;2.

Jeevanjee, N., P. Hassanzadeh, S. Hill, and A. Sheshadri, 2017: A perspective on climate model hierarchies. *J. Adv. Model. Earth Syst.*, **9 (4)**, 1760–1771, doi:10.1002/2017MS001038.

Kirtman, B. P., and E. K. Schneider, 2000: A Spontaneously Generated Tropical Atmospheric General Circulation. *J. Atmos. Sci.*, **57 (13)**, 2080–2093, doi:10.1175/1520-0469(2000)057⟨2080:ASGTAG⟩2.0.CO;2.

Korty, R. L., and T. Schneider, 2008: Extent of Hadley circulations in dry atmospheres. *Geophys. Res. Lett.*, **35 (23)**, L23 803, doi:10.1029/2008GL035847.

Levine, X. J., and T. Schneider, 2011: Response of the Hadley Circulation to Climate Change in an Aquaplanet GCM Coupled to a Simple

Representation of Ocean Heat Transport. *Journal of the Atmospheric Sciences*, **68 (4)**, 769–783, doi:10.1175/2010JAS3553.1.

Levine, X. J., and T. Schneider, 2015: Baroclinic Eddies and the Extent of the Hadley Circulation: An Idealized GCM Study. *J. Atmos. Sci.*, **72 (7)**, 2744–2761, doi:10.1175/JAS-D-14-0152.1.

Lindzen, R. S., and A. V. Hou, 1988: Hadley Circulations for Zonally Averaged Heating Centered off the Equator. *J. Atmos. Sci.*, **45 (17)**, 2416–2427, doi:10.1175/1520-0469(1988)045⟨2416:HCFZAH⟩2.0.CO;2.

Linsenmeier, M., S. Pascale, and V. Lucarini, 2015: Climate of Earth-like planets with high obliquity and eccentric orbits: Implications for habitability conditions. *Planetary and Space Science*, **105**, 43–59, doi:10.1016/j.pss.2014.11.003.

Mitchell, J. L., and J. M. Lora, 2016: The Climate of Titan. *Annual Review of Earth and Planetary Sciences*, **44 (1)**, 353–380, doi:10.1146/annurev-earth-060115-012428.

Mitchell, J. L., R. T. Pierrehumbert, D. M. W. Frierson, and R. Caballero, 2006: The dynamics behind Titan's methane clouds. *PNAS*, **103 (49)**, 18 421–18 426, doi:10.1073/pnas.0605074103.

Mitchell, J. L., and G. K. Vallis, 2010: The transition to superrotation in terrestrial atmospheres. *J. Geophys. Res.*, **115 (E12)**, E12 008, doi:10.1029/2010JE003587.

Nie, J., W. R. Boos, and Z. Kuang, 2010: Observational Evaluation of a Convective Quasi-Equilibrium View of Monsoons. *Journal of Climate*, **23 (16)**, 4416–4428, doi:10.1175/2010JCLI3505.1.

O'Neill, M. E., and Y. Kaspi, 2016: Slantwise convection on fluid planets. *Geophys. Res. Lett.*, **43 (20)**, 2016GL071 188, doi:10.1002/2016GL071188.

Pauluis, O., 2004: Boundary Layer Dynamics and Cross-Equatorial Hadley Circulation. *J. Atmos. Sci.*, **61 (10)**, 1161–1173, doi:10.1175/1520-0469(2004)061⟨1161:BLDACH⟩2.0.CO;2.

Plumb, R. A., and A. Y. Hou, 1992: The Response of a Zonally Symmetric Atmosphere to Subtropical Thermal Forcing: Threshold Behavior. *J. Atmos. Sci.*, **49 (19)**, 1790–1799, doi:10.1175/1520-0469(1992)049⟨1790:TROAZS⟩2.0.CO;2.

Polvani, L. M., and A. H. Sobel, 2002: The Hadley Circulation and the Weak Temperature Gradient Approximation. *J. Atmos. Sci.*, **59 (10)**, 1744–1752, doi:10.1175/1520-0469(2002)059⟨1744:THCATW⟩2.0.CO;2.

Privé, N. C., and R. A. Plumb, 2007a: Monsoon Dynamics with Interactive Forcing. Part I: Axisymmetric Studies. *J. Atmos. Sci.*, **64 (5)**, 1417–1430, doi:10.1175/JAS3916.1.

Privé, N. C., and R. A. Plumb, 2007b: Monsoon Dynamics with Interactive Forcing. Part II: Impact of Eddies and Asymmetric Geometries. *J. Atmos. Sci.*, **64 (5)**, 1431–1442, doi:10.1175/JAS3917.1.

Satoh, M., 1994: Hadley Circulations in Radiative–Convective Equilibrium in an Axially Symmetric Atmosphere. *J. Atmos. Sci.*, **51 (13)**, 1947–1968, doi:10.1175/1520-0469(1994)051⟨1947:HCIREI⟩2.0.CO;2.

Schneider, E. K., 1977: Axially Symmetric Steady-State Models of the Basic State for Instability and Climate Studies. Part II. Nonlinear Calculations. *J. Atmos. Sci.*, **34 (2)**, 280–296, doi:10.1175/1520-0469(1977)034⟨0280:ASSSMO⟩2.0.CO;2.

Schneider, E. K., and R. S. Lindzen, 1977: Axially Symmetric Steady-State Models of the Basic State for Instability and Climate Studies. Part I. Linearized Calculations. *J. Atmos. Sci.*, **34 (2)**, 263–279, doi:10.1175/1520-0469(1977)034⟨0263:ASSSMO⟩2.0.CO;2.

Schneider, T., 2004: The Tropopause and the Thermal Stratification in the Extratropics of a Dry Atmosphere. *J. Atmos. Sci.*, **61 (12)**, 1317–1340, doi:10.1175/1520-0469(2004)061⟨1317:TTATTS⟩2.0.CO;2.

Schneider, T., 2006: The general circulation of the atmosphere. *Annu. Rev. Earth Planet. Sci.*, **34**, 655–688.

Schneider, T., and S. Bordoni, 2008: Eddy-Mediated Regime Transitions in the Seasonal Cycle of a Hadley Circulation and Implications for Monsoon Dynamics. *J. Atmos. Sci.*, **65 (3)**, 915–934, doi:10.1175/2007JAS2415.1.

Schneider, T., and J. Liu, 2009: Formation of Jets and Equatorial Superrotation on Jupiter. *J. Atmos. Sci.*, **66 (3)**, 579–601, doi:10.1175/2008JAS2798.1.

Schneider, T., and C. C. Walker, 2006: Self-Organization of Atmospheric Macroturbulence into Critical States of Weak Nonlinear Eddy–Eddy Interactions. *J. Atmos. Sci.*, **63 (6)**, 1569–1586, doi:10.1175/JAS3699.1.

Showman, A. P., R. D. Wordsworth, T. M. Merlis, and Y. Kaspi, 2014: Atmospheric circulation of terrestrial exoplanets. *Comparative Climatology of Terrestrial Planets*, Space Science, 2nd ed., University of Arizona Press.

Singh, M. S., and Z. Kuang, 2016: Exploring the Role of Eddy Momentum Fluxes in Determining the Characteristics of the Equinoctial Hadley Circulation: Fixed-SST Simulations. *J. Atmos. Sci.*, **73 (6)**, 2427–2444, doi:10.1175/JAS-D-15-0212.1.

Singh, M. S., Z. Kuang, and Y. Tian, 2017: Eddy Influences on the Strength of the Hadley Circulation: Dynamic and Thermodynamic Perspectives. *J. Atmos. Sci.*, **74 (2)**, 467–486, doi:10.1175/JAS-D-16-0238.1.

Vallis, G. K., 2017: *Atmospheric and Oceanic Fluid Dynamics: Fundamentals and Large-Scale Circulation*. 2nd ed., Cambridge University Press.

Walker, C. C., and T. Schneider, 2005: Response of idealized Hadley circulations to seasonally varying heating. *Geophys. Res. Lett.*, **32 (6)**, L06 813, doi:10.1029/2004GL022304.

Walker, C. C., and T. Schneider, 2006: Eddy Influences on Hadley Circulations: Simulations with an Idealized GCM. *J. Atmos. Sci.*, **63 (12)**, 3333–3350, doi:10.1175/JAS3821.1.

Wang, P., and J. L. Mitchell, 2014: Planetary ageostrophic instability leads to superrotation. *Geophys. Res. Lett.*, **41 (12)**, 4118–4126, doi:10.1002/2014GL060345.

Williams, G. P., and J. L. Holloway, 1982: The range and unity of planetary circulations. *Nature*, **297 (5864)**, 295–299, doi:10.1038/297295a0.

Zalucha, A. M., R. A. Plumb, and R. J. Wilson, 2010: An Analysis of the Effect of Topography on the Martian Hadley Cells. *Journal of the Atmospheric Sciences*, **67 (3)**, 673–693, doi:10.1175/2009JAS3130.1.